

Gas and iron content of galaxy clusters

C. Chiosi*

Università di Padova, Dipartimento di Astronomia, Vicolo dell'Osservatorio 5, 35122 Padova, Italy
Max-Planck-Institut für Astrophysik, Karl-Schwarzschild-Strasse 1, 87540 Garching bei München, Germany

Received 27 March 2000 / Accepted 5 October 2000

Abstract. Up to now, many theoretical studies aimed at reproducing the total amount of iron and gas in the intra-cluster medium meet the embarrassing situation, in which if the iron content is reproduced, the gas is not. More precisely, at given iron mass, too little gas and too high Fe abundance in turn are obtained as compared to the observational data. Large dilution by primordial gas is then invoked to get rid of the difficulty. In this paper we present a new approach to this problem. Basic ingredients of the present analysis are: (i) The adoption of multi-zone models of elliptical galaxies in the framework of the super-nova driven galactic wind scheme. They yield a more realistic description of the galactic ejecta in which the effects of gradients in star formation and chemical enrichment are taken into account. (ii) The stellar initial mass function is let vary with the physical conditions of the star forming medium. More precisely, the typical mass scale of the initial mass function increases with the gas temperature. Since no cooling process exists decreasing the temperature of a galaxy's gas below the limit set by the current value of the cosmic background radiation, it immediately follows that the stellar initial mass function of proto-galaxies whose stellar activity began at high red-shift (when the CBR temperature was higher than the present-day mean temperature of molecular clouds) is different from the one in galaxies which did the same but at lower red-shift. Because of this, at given galaxy mass the ejecta are expected to depend on the red-shift. (iii) Finally, the basic assumption is made that at any time (red-shift) the mass distribution of proto-galaxies follows the Press-Schechter law holding for Dark Matter, however with masses comprised between suitable minimum and maximum values, M_L^{\min} and M_L^* , respectively, that are also varying with time and/or red-shift. This is equivalent to assume a sort of continuously varying mass function for galaxies as well. When the same input physics (stellar initial mass function and galactic ejecta) is adopted, the new method recovers previous results in literature. However, when the above three ingredients are let work simultaneously, the total amount of iron and gas are reasonably matched, a point of major difficulty in previous studies. The absolute abundance of Fe and abun-

dance ratio [O/Fe] are fully compatible with the observational determinations. However, even in this case some dilution (up to about 20%) by primordial gas (never cycled through galaxies) seems to be required. This is less than the older estimates of 65% to 90%. Finally, a simple model for the evolution of the intra-cluster medium abundances as a function of the red-shift is presented and compared with the observational data for clusters at high red-shift (up to $z \simeq 0.5$).

Key words: galaxies: clusters: general – galaxies: intergalactic medium – galaxies: evolution – galaxies: abundances

1. Introduction

Since more than two decades the intra-cluster medium (ICM) of clusters of galaxies is known to be filled by hot, metal-rich gas revealed by the X-ray emission caused by thermal bremsstrahlung at temperature of about 10^7 to 10^8 K (see Sarazin 1986). Characterizing parameters of the ICM gas are:

(i) the total mass which is of the order of one-third of the total gravitational mass in a cluster (White et al. 1993).

(ii) the abundance of iron which goes from about 1/2 solar (Rothenflug & Arnaud 1985) to 1/3 solar (Renzini 1997; Fukazawa et al. 1998).

(iii) the abundances of α -elements, which thanks to ASCA have been put on a more firm ground. Before ASCA, spectroscopic measures of Si and S were known only for two clusters (Perseus and A576) indicating about solar values (Mushotzky et al. 1981; Rothenflug et al. 1984) or higher than solar (Canizares et al. 1988). More recent data from ASCA by Mushotzky et al. (1996) yield $[\frac{\alpha}{Fe}] \simeq 0.2 \pm 0.3$ or in the case of oxygen $[\frac{O}{Fe}] \simeq 0.48_{-0.55}^{+0.24}$, which means, considering the uncertainty, a marginal over-abundance of oxygen relative to iron. The ratio [Si/Fe] derived from Mushotzky's et al. (1996) data is $[\frac{Si}{Fe}] \simeq 0.37_{-0.35}^{+0.17}$ in agreement with the analysis by Fukazawa et al. (1998). Ishimaru & Arimoto (1997) and Arimoto et al. (1997) argue that considering the uncertainties all the data are consistent with the solar value.

(iv) Finally, the ASCA study by Finoguenov et al. (1999) of heavy element distribution in clusters of galaxies indicates that

Send offprint requests to: chiosi@pd.astro.it

* Visiting Scientist, Max-Planck-Institut für Astrophysik, Garching bei München, Germany

the total abundance of Fe decreases significantly with cluster radius, while the Si abundance is either flat or decreases less rapidly, resulting into an increasing [Si/Fe] ratio with radius. See also the recent analysis by White (1999) and White & Dupke (2000).

It is widely accepted that the ICM metals have been processed in galaxies and subsequently either ejected or stripped away. Indeed, the super-nova driven galactic wind (SDGW) model of Larson (1974) is the favored mechanism for ejecting heavy elements (Matteucci & Vettolani 1988; David et al. 1991; Ciotti et al. 1991; Mihara & Takahara 1994; Bressan et al. 1994; Matteucci & Gibson 1995; Elbaz et al. 1995; Tantalò et al. 1996, 1998; Gibson & Matteucci 1997; Chiosi et al. 1998; Martinelli et al. 1998), although the ram pressure stripping of the enriched interstellar medium during the initial phase of star formation cannot be excluded (Sarazin 1979). We recall, however, that arguments are given by White (1991) and Renzini et al. (1993) against the stripping scenario.

By integrating the mass of metals ejected by ellipticals of different initial mass over the Schechter luminosity function with faint end slope $\beta = -1.25$, Matteucci & Vettolani (1988, MV88) first tried to account for the mass of iron observed in the ICM. However, two drawbacks of their early study were (i) the overproduction of iron with respect to α -elements, i.e. $[\alpha/\text{Fe}] \leq 0$; (ii) recovery of the total iron mass, but much lower total gas mass predicted by the models with respect to observations (only 10%–20%). *The conclusion was that the bulk of the gas is of primordial origin.*

Attempts to get the right abundance ratios were by Arnaud et al. (1992) and Matteucci & Gibson (1995, MG95) who adopted an initial mass function (IMF) of the stars in galaxies with a flatter slope than the Salpeter value ($x \simeq 1$ instead of 1.35). The two studies differ for some aspects of the galaxy models but lead to similar results. Elbaz et al. (1995) postulated the existence of a bimodal IMF, i.e. a first generation made only by massive stars followed by others with the standard IMF. This suggestion was questioned by Gibson (1996) who claimed that galaxies with a bimodal IMF at the early epochs would have present-day photometric properties inconsistent with observational data.

Attempts to get the required amount of total gas were by Trentham (1994), Nath & Chiba (1995) and Gibson & Matteucci (1997, GM97). The novelty was the adoption of a much steeper slope of the Schechter function in the range of dwarf galaxies, that appeared to be more consistent with observational luminosity functions in galaxy clusters (De Propris et al. 1995 and references). The idea was that if the slope over there is $\beta \simeq -2$ and dwarf galaxies eject 8% to 30% of their initial total mass in the form of gas after the first burst of star formation, the dwarf galaxies can solve the problem of the present day ICM gas. The most systematic analysis of this topic in the context of the SDGW model is by Gibson & Matteucci (1997), who came to the following conclusion: *“even assuming an extreme scenario in which all the gas returned by dying stars is ejected continuously to the ICM, neither the giant ellipticals nor the dwarf spheroidals (nor their sum, for that matter) can be responsible for all the gas and iron observed in the ICM of galaxy clus-*

ters, provided that we insist that the resultant galaxies reflect the photochemical properties of present-day systems. A large fraction of the gas must be primordial.”

The latest study on the subject is by Martinelli et al. (1999, MMC99) who made use of one-zone and multi-zone SDGW models of elliptical galaxies (Martinelli et al. 1998; Tantalò et al. 1998, and below for more details) and studied the dependence of the ICM abundances with red-shift. The key idea is that the multi-zone models suffer from galactic winds over longer periods of time as compared to the one-zone models. Specifically, the outermost regions of the former experience early galactic winds (and little star formation and chemical enrichment in turn) whereas their innermost regions keep active star formation for longer times, produce more metals, and finally eject less gas. With the aid of these models, they estimate the abundance and abundance ratio [Fe/H] and [O/Fe] of the ICM. In brief, (i) [Fe/H] and [O/Fe] decreases and increases, respectively, with the red-shift in a way that depends on the galaxy model and the cosmological parameters used to link galaxy lifetime to red-shift; (ii) at red-shift $z=0$ the one-zone galaxies predict for the ICM [Fe/H] from 0.22 to 0.36 and [O/Fe] from 0.27 to 0.33 depending on the cosmological model, whereas the multi-zone galaxies yield [Fe/H] from 0.75 to 0.9 and [O/Fe] from -0.12 to -0.04 . While the abundance ratios [O/Fe] of both cases are within the observational determination, the abundances [Fe/H] are definitely too large and admittedly require large dilutions by primordial gas. No information is given about the total amount of gas expected in the ICM.

In this paper, we intend to reconsider the whole problem in the light of several major changes in galaxy models and their ejecta. Firstly, we adopt galaxy models with a radial dependence of star formation and chemical enrichment. Secondly, we explore the possibility that the IMF in early stages was different from the one we are familiar with in the solar vicinity, and explore the consequences of it. Though reminiscent of the suggestion made by Elbaz et al. (1995), the kind of IMF we are going to apply to model galaxies is much more articulated than the simple bimodal prescription. Furthermore, it has already been successfully applied by Chiosi et al. (1998) to discuss the color-magnitude relation (CMR) and tilt of the fundamental plane (FP) of elliptical galaxies. Thirdly, we follow a different method to evaluate the total amounts of gas and elemental species (iron) injected by galaxies into the ICM. Finally, we present a simple model for the chemical enrichment of the ICM.

In Sect. 2 we present the basic data to interpret. In Sect. 3 we shortly discuss the reasons why the standard galaxy models fail. In Sect. 4 we briefly argue about the possibility that in the past the stellar IMF has been different from the one we see today. In Sects. 5 and 6 we present new galaxy models with radial gradients in mass density and star formation and stellar IMF changing with the physical conditions of the star forming medium. In Sect. 7 we present the ejecta of various elemental species from galaxies formed at different red-shift. In Sect. 8 we describe the method we have adopted to model the ICM gas and metal contents, and in Sect. 9 we define the normalization procedure. In Sect. 10 we present some preliminary tests

Table 1. The logarithm of the total masses of Gas and Iron in solar units, the mass abundance of Fe with respect to the Sun, and the cluster red-shift.

| Cluster Name | M_g | M_{Fe} | $\frac{X_{Fe}}{X_{Fe,\odot}}$ | z |
|----------------|-------|----------|-------------------------------|--------|
| A426 (Perseus) | 14.5 | 11.3 | 0.241 | 0.018 |
| A1656 (Coma) | 14.6 | 11.5 | 0.303 | 0.022 |
| A2199 | 14.2 | 11.1 | 0.301 | 0.030 |
| Virgo | 13.3 | 10.2 | 0.303 | 0.0036 |

Table 2. Old theoretical models. The first column lists either the cluster richness or the logarithm of the total V luminosity L_V in solar units. The second and third columns list the logarithm of gas and iron mass in solar units. See the text for the sources of data.

| L_V/Rich | M_{Fe} | M_g | Source |
|-------------------|----------|-------|-----------|
| Rich | 11.40 | 13.30 | MV88 |
| Poor | 10.10 | 12.00 | |
| Rich | 10.64 | 12.68 | MG95 |
| Poor | 9.07 | 11.23 | |
| 11 | 8.80 | 11.40 | GM97 Min |
| 12 | 9.80 | 12.40 | |
| 11 | 9.37 | 11.88 | GM97 Max |
| 12 | 10.40 | 12.88 | |
| 11 | 9.25 | 11.80 | GM97 Stan |
| 12 | 10.28 | 12.80 | |

aimed at recovering the results of previous studies. In Sect. 11 we discuss the final models and in Sect. 12 the present-day abundances of iron and oxygen in the ICM. In Sect. 13 we present a simple model for the chemical evolution of the ICM and compare the theoretical results with observational data for clusters at different red-shift. Finally, in Sect. 14 we draw some general conclusions and remarks.

2. The data

In this section we shortly present the data we want to reproduce, i.e. the total amounts of iron and gas estimated for several galaxy clusters of different richness. The data are the same as those examined by MV88. They are listed in Table 1 together with an estimate of the iron abundance relative to the solar value $X_{Fe}/X_{Fe,\odot}$ and the red-shift z , Columns (4) and (5), respectively.

Throughout this paper, for the iron abundance of the Sun we adopt the photospheric determination by Anders & Grevesse (1989) $X_{Fe,\odot} = 4.68 \times 10^{-5}$ by number or $X_{Fe,\odot} = 2.62 \times 10^{-3}$ by mass. Column (4) of Table 1 lists the iron abundance by mass of the clusters under examination. The use of the solar Fe abundance based on meteoritic data that is sometimes preferred by other authors would not significantly change the results of this study.

The solutions found by MV88, MG95 and GM97 are summarized in Table 2.

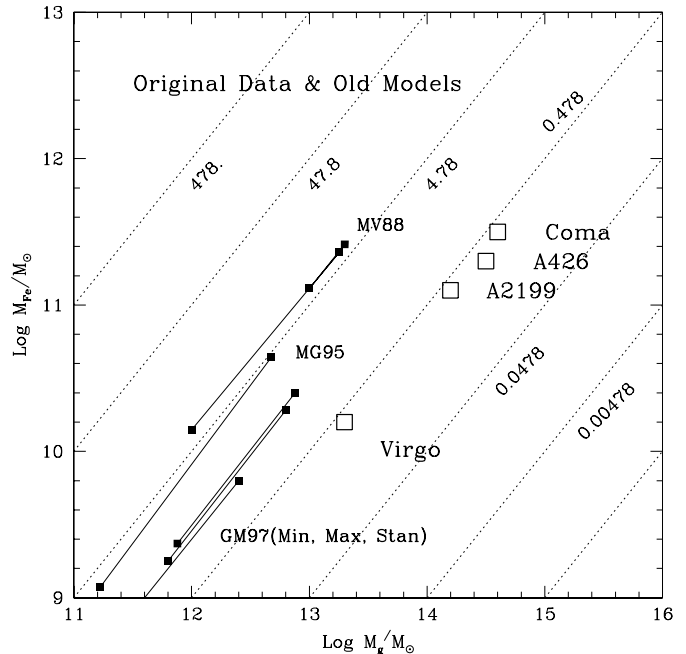


Fig. 1. Observational data and old theoretical predictions. The open squares are the data for four galaxy clusters of Table 1 as indicated. The solid lines are the theoretical predictions by MV88, MG95 and GM97. Finally, the thin dotted lines are the loci of constant abundance $X_{Fe}/X_{Fe,\odot}$ as indicated

Finally, the observational data (open squares) and theoretical results (solid lines) are plotted in Fig. 1 correlating on a logarithmic scale the total gas mass to the total iron mass (both in solar units).

The advantage of this diagram is that loci of constant abundance of any elemental species (Fe in this case) are straight lines of slope one (they are shown in Fig. 1 by the thin dotted lines labelled by the corresponding abundance with respect to the Sun).

From the position of the four clusters under examination we learn immediately that (i) there is a small scatter in abundance; (ii) Coma, Virgo and A2199 have the same abundance ($X_{Fe}/X_{Fe,\odot} \simeq 0.3$), A426 is slightly less iron-rich ($X_{Fe}/X_{Fe,\odot} \simeq 0.2$).

Looking at the theoretical results and observational data shown in Fig. 1, the difficulty in question is soon evident. Models matching the total iron mass are too short in the total gas mass. Equivalently, all models predict Fe abundances of the ICM that are significantly higher, up to more than a factor of ten in some cases, than the observational determination.

In addition, it is worth noticing that in the course of the years the situation instead of improving got worse. As a matter of facts, while the MV88 theoretical results were appropriate for the Fe mass and off by about a factor of ten for the gas mass, the results of MG95 are off for both quantities (indeed they marginally match only the Fe content in Virgo). The same considerations apply to the models by GM97.

3. Why do the standard models fail?

Before giving up with the idea that all the gas and metals we see in clusters are of galactic origin, i.e. processed by stars inside galaxies and subsequently expelled by these via SN powered galactic winds, let us pose the general question as to why standard models of galaxies fail to supply enough gas and/or metals.

Most of the galaxy models used in so far share the following assumptions and/or properties:

(i) A galaxy is conceived as single entity of initial total baryonic mass M_T embedded in a halo of Dark Matter of mass M_D and radius R_D , chemically behaving as a Closed-Box model. The gas is turned into stars at a suitable rate till the energy deposit by super-nova explosions and stellar winds overwhelms the gravitational energy. When this happens, the gas is supposed to flow out freely (galactic wind) and star formation to halt. For more details see Bressan et al. (1994). Whether the galactic wind occurs instantaneously or over a finite time scale is of marginal relevance here because the results would be nearly the same (see GM 1997).

(ii) The star formation rate (SFR) is usually expressed as a power of the gas mass M_g

$$\frac{dM_g}{dt} = \nu M_g^\kappa \quad (1)$$

with $\kappa = 1$. The parameter ν is derived from imposing some significant constraint, for instance ensuring that the CMR of elliptical galaxies is recovered (see Bressan et al. 1994).

(iii) In most cases, the classical IMF by Salpeter (1955) is adopted to calculate the mass distribution of stars and the chemical yields of elemental species. This IMF (hereinafter the standard case) is

$$\frac{dN}{d\log M} \propto M^{-x} \quad (2)$$

where $x = 1.35$ and the proportionality constant is fixed by a normalization procedure over a suitable mass interval, usually from $M_l = 0.1 M_\odot$ to $M_u = 100 M_\odot$. The IMF in usage is particularly relevant because it drives the efficiency of gas recycling and chemical enrichment in turn. Suffice it to mention that massive stars (say above $2 M_\odot$) re-eject a large fraction of their mass over a time scale short compared to the typical galaxy lifetimes (say 12–13 Gyr), whereas low-mass stars (say smaller than about $1.5 M_\odot$) do the same over a time scale comparable or longer than the galaxy ages. In the cases in which IMFs different from the Salpeter law have been adopted, the major changes were limited to the slope in the upper mass range (see for instance the models in MG95 and GM97). However, as far as chemical enrichment is concerned, recalling the definition of yield per stellar generation (Tinsley 1980), the slope of the IMF in the low-mass end is even more important than that of the high mass one.

(iv) The coupling of the above SFR and IMF with the closed-box description and the current efficiency of super-nova heating, implies that almost all gas is turned into stars before the onset of galactic winds. Good examples are the closed-box models

of Bressan et al. (1994), designed to fit the CMRs of Virgo and Coma galaxies. For instance their $5 \times 10^{10} M_\odot$ galaxy at the age $t_{\text{gw}} = 0.08$ Gyr at which galactic winds occur has the following fractionary masses of gas and stars: $M_g/M_T = 0.08$ and $M_s/M_T = 0.90$. Similarly, their $1 \times 10^{12} M_\odot$ object has $t_{\text{gw}} = 0.08$ Gyr, $M_g/M_T = 0.26$ and $M_s/M_T = 0.73$. It is worth mentioning that similar values are also found with the so-called *infall*-models by Tantalò et al. (1996) aimed at solving the G-dwarf analog seen in the UV spectra of elliptical galaxies¹.

(v) Finally, all SDGW models with the standard Salpeter IMF cannot explain the observed trend in the enhancement of α -elements as a function of the galaxy luminosity (mass): brighter (more massive) galaxies seem to be more α -enriched than the fainter (less massive) ones (see Matteucci 1997 for a recent review on the subject). Indeed these models predict the opposite as already pointed out in a number of studies (Bressan et al. 1996; Matteucci 1997; Chiosi et al. 1998; Chiosi 2000).

Among the above remarks two points are relevant here. First, the ICM gas and metal content problem has been addressed using galaxy models that are not fully consistent with observational data, second models of this type are not able to give back to the ICM enough gas because they convert too large a fraction of this into stars.

There is at least one aspect of the problem in which even the standard models could be improved, i.e. the adoption of the one-zone closed-box description. Elliptical galaxies indeed have spatial gradients in luminosity, mass density, and colors, which likely mirror spatial gradients in SFR, metallicity and other properties. An attempt to deal with all this in a simple fashion are the multi-zone models by Martinelli et al. (1998) and Tantalò et al. (1998). The most relevant result of this type of models is that the outermost regions of galaxies experience very early galactic winds, whereas the innermost ones keep forming stars for much longer times. Therefore, in the external regions of a galaxy, a larger fraction of the available gas is given back to the ICM with mild chemical enrichment. Only a small fraction is turned into stars. The opposite holds for the innermost regions. Despite the crudeness of the multi-zone approach, the results for the final outcome are not bad compared with observations (see Martinelli et al. 1998, and Tantalò et al. 1998 for all details). Multi-zone models have already been used by Martinelli et al. (1999) to study the ICM problem.

The other important ingredient to play with is the IMF of the first stars formed in galaxies. The subject has been addressed by Chiosi et al. (1998) who proposed models of ellipticals making

¹ We like to comment here on the remark made by Vazdekis et al. (1996), Worthey et al. (1996) and Larson (1998) that *infall models cannot be applied to elliptical galaxies because there is less time for infall to be effective and elliptical galaxies in clusters lose rather than accrete large amounts of gas*. This way of reading the infall models by Tantalò et al. (1996) is misleading. Indeed the authors named infall models those in which at very early epochs the collapse time-scale and the star formation time scale were comparable, so that as a net result the SFR instead of being exponentially declining as in the closed box description, started small, rose to a maximum and then declined. All this happened before galactic winds took place.

use of an IMF sensitive to the physical conditions of the star forming medium. No use of these models has been made in so far to tackle the problem of the ICM.

4. The IMF of the first stars

Is there any plausible reason why the first generations of stars in primeval galaxies had an IMF different from the one we see today and even more important the classical Salpeter law?

The whole subject has recently been discussed by Larson (1998) to whom the reader should refer for details. Suffice it to recall a few relevant points:

(i) The present-day IMF in the solar vicinity can be described by a declining power law for masses above $1 M_{\odot}$, i.e. the classical Salpeter (1955) law of relation (2), flattening below $\simeq 0.5 M_{\odot}$, and possibly even declining below $\simeq 0.25 M_{\odot}$ (Scalo 1998).

The above trends are suitably represented by the following analytical relationship

$$\frac{dN}{d\log M} \propto M^{-x} \exp\left(-\frac{M_s}{M}\right) \quad (3)$$

where M_s is a characteristic mass-scale. With the above representation, the IMF approaches the Salpeter (1955) law at large masses, peaks at $M_p = M_s/x$, and falls exponentially at lower masses.

(ii) In this context, the whole problem is reduced to understanding whether x and M_s have always been the same or they have changed with time and hence physical conditions of the medium.

(iii) The mass scale M_s might be related to a fundamental scale in the star forming process such as the Jeans mass (Larson 1995). The Jeans mass is proportional to the pressure and temperature in the star forming clouds, i.e. $M_s \propto T^2 P^{-1/2}$, where the temperature is the dominant parameter. This is controlled by the balance between heating by external radiation fields and cooling by line emission from atoms and molecules and thermal emission from dust. More intense radiation fields and lower heavy elements abundances would imply higher temperatures and larger M_s unless there is a sufficiently large compensating increase in pressure. *How were temperature and pressure at the early times?* While there are no compelling arguments for the pressure in star-forming clouds has to be much higher at early times, there are several reasons for the temperature has indeed to be higher. Firstly, the cosmic background radiation temperature T_{CBR} , which is the minimum possible cloud temperature, scales with red-shift as $T_{\text{CBM}} = 2.73(1+z)$, and it becomes higher than the present day temperature in molecular clouds ($\simeq 10$ K) at red-shift greater than about 2. Secondly, at early stages the abundance of heavy elements is lower, which implies lower cooling efficiencies per given heating rate. Finally, the heating rate was certainly higher in the far past because of the intense field radiation and likely strong stellar activity (supernova explosions, stellar winds, cosmic rays, etc.)

(iv) The arguments above suggest that at early stages M_s and M_p in turn were significantly skewed towards relatively

high masses. It is worth clarifying here that strong effects would result even by changing M_s by a modest amount. If the present-day value in the solar vicinity is such that $M_p \simeq 0.20 M_{\odot}$, an increase of M_p up to $1 M_{\odot}$ would significantly change the IMF (see below). As far as the slope of the IMF is concerned very little can be said. At early epochs the mean slope above M_p was likely flatter than today.

Is there any theoretical IMF having the kind of behavior we have discussed in so far?

Padoan et al. (1997, PNJ97), making use of a statistical description of the density field emerging from randomly forced supersonic flows in star forming regions, presented hydrodynamical simulations of supersonic flows and found that very large density contrasts can develop with log-normal probability distribution. With the aid of these, they derived a theoretical IMF which depends on the physical conditions of the star forming gas, i.e. temperature, density and velocity dispersion. The IMF by PNJ97 is

$$\int_0^{\infty} \phi(M) dM = \int_0^{\infty} \frac{2\Theta^2}{(2\pi\sigma^2)^{0.5}} M^{-3} \exp\left[-0.5\left(\frac{2\ln M - \Lambda}{\sigma}\right)^2\right] dM = 1 \quad (4)$$

where $\Lambda = 2 \ln \Theta + 0.5\sigma^2$, $\Theta = 1.2 \times (T/10)^{1.5} \times (n/1000)^{-0.5}$, and $\sigma^2 = \ln[1 + 0.36(M_a^2 - 1)]$; σ is the standard deviation of the number density distribution in the field with respect to the mean, M_a^2 is the square of the Mach number $M_a^2 = (\Sigma_g/v_s)^2$, T is the temperature in K, n is the number density in cm^{-3} , v_s the sound velocity, and Σ_g the velocity dispersion of the gas (in km/s).

This IMF has a long tail at high masses, an exponential cutoff at the smallest masses, a characteristic peak mass

$$M_p \simeq 0.2 M_{\odot} \times (T/10)^2 \times (n/1000)^{-0.5} \times (\Sigma_g/2.5)^{-1} \quad (5)$$

and a slope continuously varying with the mass. The IMF gets flatter and M_p gets higher at increasing temperature or decreasing density and velocity dispersion.

Although the mass integration limits of the IMF by PNJ97 are from 0 to ∞ , for the purposes of practical use we integrate the IMF from $M_l = 0.1 M_{\odot}$ to $M_u = 100 M_{\odot}$. This approximation is valid as long as $M_p \ll M_u$, which applies to all reasonable values of the gas temperature, density and velocity dispersion.

It might be a mere coincidence but the IMF by PNJ97 has the kind of functional dependence on the star mass advocated by Larson (1998) and given by Eq. (3). This is best shown in Fig. 2, where we plot the IMF by PNJ97 for the typical conditions of molecular clouds in the Solar Vicinity, characterized by the set of parameters $T = 10$ K, number density $n = 1000 \text{ cm}^{-3}$ and $\Sigma_g = 2.5 \text{ km s}^{-1}$ and the Larson IMF given by Eq. (3) with $M_s \simeq 0.6 M_{\odot}$ and $M_p \simeq 0.25 M_{\odot}$. Both IMFs have been re-normalized to numerically coincide at M_p for the sake of representation.

5. Multi-zone models with variable IMF

In this study we make use of the SDGW multi-zone spherically symmetric models developed by Tantaló et al. (1998, TCB98) in which radial gradients in the gas and mass densities and star formation rate are taken into account. This same type of models have already been adopted by Chiosi et al. (1998, CBPT98) to study the effect of the IMF by PNJ97.

For the sake of simplicity and better understanding of the role played by the sole IMF, the closed-box formulation (no infall of primordial gas) is adopted, however the contribution of dark matter to the total gravitational potential of the galaxy to evaluate the time t_{gw} of galactic wind is taken into account.

The equations governing gas consumption and chemical enrichment are the same as in CBPT98 and/or TCB98 and will not be repeated here.

The models are written introducing in each spherical shell the density of total baryonic mass ρ , the density of gas ρ_g and the density of stars ρ_s and imposing that the present-day mass density profile follows the Young (1976) law.

Basing on the analysis by TCB98 and for the purposes of the present study a three-zone description is sufficient. Given a spherical proto-galaxy of total gas mass M_L , total radius R_T and effective radius R_e , three typical zones are recognized:

(i) The sphere inside the effective radius R_e , in which most of the gas is turned into stars and metals are made.

(ii) The intermediate corona of thickness ΔR comprised between R_e and $2 \times R_e$, in which only a fraction of the gas is turned into stars and yet significant chemical enrichment occurs.

(iii) Finally, the outer corona of thickness ΔR comprised from $2 \times R_e$ to R_T (total radius), in which very small star formation and metal enrichment take place. The gas of this region is essentially ejected back into the intergalactic medium with no chemical processing.

By definition (see TCB98 for all details), the baryonic mass contained in each zone has fixed values, namely $M(R_e) = 0.414 \times M_L$, $M(\Delta R)_i = 0.189 \times M_L$, and $M(\Delta R)_e = 0.397 \times M_L$.

An important point to remember is that, owing to the occurrence of galactic winds, only part of the initial proto-galactic mass M_L will survive as a galaxy made of stars. The mass of this is given by

$$\begin{aligned} M_G &= M_s(R_e) + M_s(\Delta R)_i + M_s(\Delta R)_e \\ &= M_L - M_g(R_e) - M_g(\Delta R)_i - M_g(\Delta R)_e \end{aligned} \quad (6)$$

where $M_s(R_e)$, $M_s(\Delta R)_i$, and $M_s(\Delta R)_e$ are the masses in stars of the three regions, whereas $M_g(R_e)$, $M_g(\Delta R)_i$, and $M_g(\Delta R)_e$ are the same but for the expelled gas.

Star Formation. The SFR is always the Schmidt law but expressed as

$$\frac{d\rho_g(t)}{dt} = \nu \rho_g(t)^\kappa \quad (7)$$

where $\kappa = 1$ and ν is the specific efficiency. This is calibrated to reproduce the CMR of elliptical galaxies in Virgo and Coma (Bower et al. 1992).

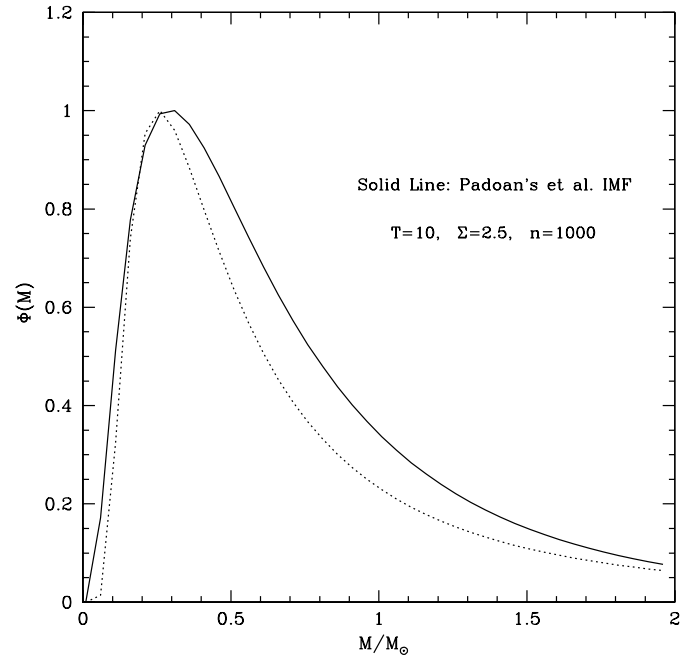


Fig. 2. The stellar IMF. The thick solid line is the IMF by PNJ97 for a typical molecular cloud in the Galactic Disk for which the following parameters are assumed: $T = 10$ K, number density $n = 1000 \text{ cm}^{-3}$ and $\Sigma_g = 2.5 \text{ km s}^{-1}$. The thin dotted line is the Larson (1998) IMF for the Solar Vicinity according to Eq. (3), with $M_s \simeq 0.6 M_\odot$ and $M_p \simeq 0.25 M_\odot$.

Energy balance. In order to calculate the IMF one has to know the density, temperature and velocity dispersion Σ_g of the star forming gas. This requires to model the thermal response of gas to supernova and stellar winds heating rate and cooling rate by radiative processes.

Following CBPT98 to whom the reader should refer for all details, the task is achieved by solving the energy equation

$$\frac{dE}{dt} = H_C + H_R + H_M - \frac{\Lambda_c}{\rho_g} \quad (8)$$

where $E(T, \rho_g, t)$ is the energy input per unit mass, $H_R(T, \rho_g, t)$, H_M and H_C are the heating rates (per unit mass) of radiative, mechanical, and collapse origin, respectively, and $\Lambda_c(T, \rho_g, t)$ is the cooling rate (in units of $\text{ergs cm}^{-3} \text{ s}^{-1}$).

(i) The term H_C is related to the very initial period of galaxy formation (see CBPT98 for details), it provides the initial gas temperature, but has marginal effects on the subsequent evolution of the galactic models.

(ii) The term H_R is made of the contribution from supernova explosions (both Type I and II) and stellar winds from massive stars (only 0.3 of their total kinetic energy is used), and a small fraction (0.01) of the ultraviolet flux from massive stars.

(iii) The term H_M owes its origin to mechanical interactions of different nature among gas clouds, such as collisions, shock waves, friction, cosmic rays, etc. Looking at cloud-cloud collisions as the primary source, this term is expressed by $H_M = \eta_M \times \Sigma_g^2 / t_{\text{ff}}$ where η_M is an efficiency parameter masking the real complexity of the overall problem. H_M plays the

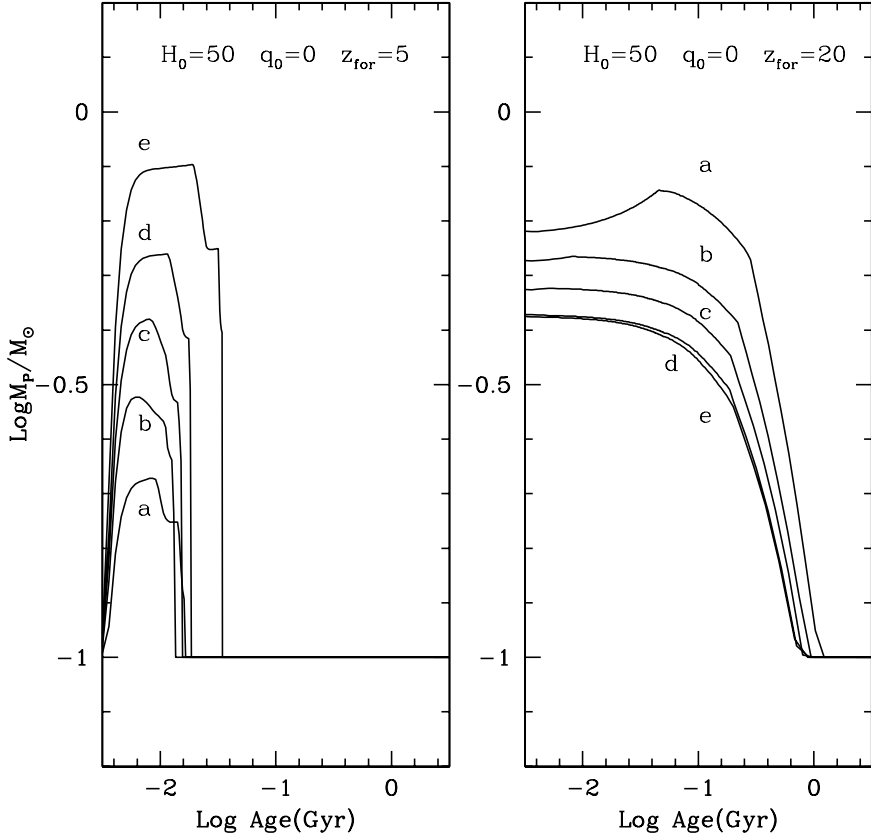


Fig. 3. M_p as function of the age for the central sphere $M(R_e)$ of galaxies of different mass M_L as indicated by the lower case letters: $1 \times 10^8 M_\odot$ (a), $1 \times 10^9 M_\odot$ (b), $1 \times 10^{10} M_\odot$ (c), $1 \times 10^{11} M_\odot$ (d), $1 \times 10^{12} M_\odot$ (e). The left panel is for $z_{\text{for}} = 5$, whereas the right panel is for $z_{\text{for}} = 20$. In both cases $H_0 = 50$ km/s/Mpc and $q_0 = 0$ as displayed

dominant role because it ultimately sets the minimum temperature attainable by the collapsing gas. In other words, this parameter somehow controls the value of M_p : the lower η_M the lower is M_p . As amply described in CBTP98, to whom the reader should refer for details, η_M was fixed by imposing that the resulting galaxy models were able to simultaneously match the CMR and tilt of the Fundamental Plane of elliptical galaxies. All the models presented here are calculated with $\eta_M = 2 \times 10^{-6}$.

Radiative and molecular cooling. The cooling term $\Lambda_c(T, \rho_g, t)$ is derived from literature data (see CBTP98 for the references). The effect of different metallicities is taken into account.

The thermal model. At each time step Δt the energy equation is solved assuming that heating-expansion and cooling-contraction of gas occur at constant pressure until equilibrium values for the temperature and density are reached. They determine the Jeans mass above which gas clouds are gravitationally unstable, and fix the velocity dispersion Σ_g of the gas clouds via the assumption of energy equi-partition. From now on the unstable gas clouds are conceived as thermally decoupled from the surrounding medium (H_R is switched off, whereas H_M is retained) and let reach the collapse temperature and density.

In any case, the gas temperature cannot fall below the current value of the CBR

$$T_{\text{CBR}}[z(t)] = 2.73 \times [1 + z(t)] \quad (9)$$

where $z(t)$ is the red-shift corresponding to the galactic age t .

6. Models with different z_{for}

It was already clear from the CBPT98 results that by changing the red-shift of galaxy formation, galaxies of the same total mass would form stars and evolve in different fashion thanks to the different minimum gas temperature at the very early stages. Indeed a galaxy of any mass formed at higher red-shift can expel more gas than an object of the same mass formed at lower red-shifts.

To follow up with this idea, we have calculated model galaxies with different values of z_{for} . For the sake of simplicity we have adopted $H_0 = 50 \text{ km s}^{-1} \text{ Mpc}^{-1}$ and $q_0 = 0$ to fix the maximum age of a galaxy.

The main physical quantities characterizing a model and its structure are summarized in Table 3 limited to the central sphere and intermediate shell. For each zone we list the maximum values of M_p^{max} and corresponding gas temperature T_g^{max} reached during the early stages, the age of the local galactic wind, the fractionary masses of gas and stars, and the mean metallicity that are attained at this stage².

To illustrate the effect of z_{for} on the minimum gas temperature and M_p in turn, we display in Fig. 3 the variation of M_p in

² In order to avoid misunderstanding, the fractionary masses of gas and stars refer to the total mass in the zone and not the total mass of the proto-galaxy. Therefore they must be suitably rescaled. For instance, if the central region has a fractionary mass of stars q_s , the real mass in solar units is $M_s = q_s \times M(R_e) = q_s \times 0.414 \times M_L$. The same for the gas and all other regions.

Table 3. Basic data of the models both for the central sphere inside $M(R_e)$ and the intermediate shell $M(\Delta R)_i$. The correspondence between z_{for} and galaxy age T_G is for $H_0 = 50 \text{ km/s}^{-1}/\text{Mpc}$ and $q_0 = 0$.

| M_L | Inner Sphere | | | | | | Intermediate Shell | | | | | |
|--|--------------------|--------------------|-----------------|----------------------|----------------------|--------------------------------------|--------------------|--------------------|-----------------|-----------------------------|-----------------------------|---------------------|
| | T_g^{max} | M_p^{max} | t_{gw} | $\frac{M_g}{M(R_e)}$ | $\frac{M_s}{M(R_e)}$ | $\langle Z \rangle$ | T_g^{max} | M_p^{max} | t_{gw} | $\frac{M_g}{M(\Delta R)_i}$ | $\frac{M_s}{M(\Delta R)_i}$ | $\langle Z \rangle$ |
| Red-shift of formation $z_{\text{for}} = 5$; | | | | | | Galaxy age $T_G = 16.45 \text{ Gyr}$ | | | | | | |
| 1e6 | 19.1 | 0.100 | 0.82 | 0.002 | 0.995 | 0.0002 | 24.0 | 0.825 | 0.01 | 0.984 | 0.016 | 0.0001 |
| 1e7 | 21.7 | 0.100 | 0.90 | 0.002 | 0.991 | 0.0003 | 26.0 | 1.280 | 0.06 | 0.582 | 0.416 | 0.0005 |
| 1e8 | 25.5 | 0.211 | 0.86 | 0.005 | 0.974 | 0.0015 | 29.9 | 1.790 | 0.05 | 0.621 | 0.373 | 0.0021 |
| 1e9 | 29.5 | 0.300 | 0.82 | 0.011 | 0.942 | 0.0059 | 33.8 | 2.350 | 0.07 | 0.582 | 0.403 | 0.0057 |
| 1e01 | 33.9 | 0.417 | 0.74 | 0.019 | 0.907 | 0.0155 | 37.9 | 3.010 | 0.06 | 0.581 | 0.390 | 0.0025 |
| 1e11 | 38.0 | 0.549 | 0.52 | 0.053 | 0.858 | 0.0295 | 46.5 | 5.270 | 0.09 | 0.630 | 0.280 | 0.0012 |
| 1e12 | 42.6 | 0.801 | 0.39 | 0.123 | 0.770 | 0.0511 | 53.9 | 8.340 | 0.01 | 0.979 | 0.021 | 0.0001 |
| Red-shift of formation $z_{\text{for}} = 10$; | | | | | | Galaxy age $T_G = 17.98 \text{ Gyr}$ | | | | | | |
| 1e6 | 30.0 | 0.100 | 0.75 | 0.003 | 0.993 | 0.0002 | 30.5 | 0.105 | 0.02 | 0.866 | 0.134 | 0.0001 |
| 1e7 | 30.0 | 0.146 | 0.77 | 0.004 | 0.985 | 0.0007 | 29.2 | 0.954 | 0.05 | 0.670 | 0.316 | 0.0046 |
| 1e8 | 31.0 | 0.158 | 0.71 | 0.012 | 0.955 | 0.0025 | 29.7 | 0.839 | 0.05 | 0.694 | 0.284 | 0.0080 |
| 1e9 | 32.0 | 0.165 | 0.79 | 0.016 | 0.922 | 0.0083 | 32.1 | 0.928 | 0.06 | 0.680 | 0.280 | 0.0029 |
| 1e10 | 33.2 | 0.170 | 0.63 | 0.031 | 0.892 | 0.0168 | 35.8 | 1.200 | 0.06 | 0.692 | 0.270 | 0.0010 |
| 1e11 | 35.0 | 0.195 | 0.43 | 0.080 | 0.837 | 0.0272 | 42.6 | 1.860 | 0.08 | 0.692 | 0.265 | 0.0020 |
| 1e12 | 40.7 | 0.316 | 0.39 | 0.127 | 0.769 | 0.0446 | 52.6 | 3.610 | 0.01 | 0.984 | 0.016 | 0.0000 |
| Red-shift of formation $z_{\text{for}} = 15$; | | | | | | Galaxy age $T_G = 18.61 \text{ Gyr}$ | | | | | | |
| 1e6 | 36.5 | 0.319 | 0.57 | 0.011 | 0.980 | 0.0003 | 43.7 | 2.240 | 0.01 | 0.919 | 0.081 | 0.0001 |
| 1e7 | 40.0 | 0.446 | 0.63 | 0.022 | 0.934 | 0.0030 | 43.7 | 2.000 | 0.01 | 0.910 | 0.088 | 0.0002 |
| 1e8 | 43.0 | 0.367 | 0.70 | 0.024 | 0.905 | 0.0077 | 43.7 | 1.755 | 0.05 | 0.755 | 0.215 | 0.0132 |
| 1e9 | 43.3 | 0.313 | 0.60 | 0.039 | 0.871 | 0.0178 | 43.7 | 1.555 | 0.06 | 0.754 | 0.214 | 0.0020 |
| 1e10 | 43.4 | 0.275 | 0.25 | 0.197 | 0.741 | 0.0206 | 43.7 | 1.380 | 0.06 | 0.753 | 0.213 | 0.0026 |
| 1e11 | 43.5 | 0.247 | 0.22 | 0.271 | 0.660 | 0.0292 | 43.7 | 1.230 | 0.09 | 0.752 | 0.211 | 0.0027 |
| 1e12 | 43.6 | 0.245 | 0.22 | 0.322 | 0.595 | 0.0408 | 43.7 | 1.680 | 0.01 | 0.984 | 0.016 | 0.0001 |
| Red-shift of formation $z_{\text{for}} = 20$; | | | | | | Galaxy age $T_G = 18.91 \text{ Gyr}$ | | | | | | |
| 1e6 | 43.4 | 0.548 | 0.43 | 0.033 | 0.953 | 0.0005 | 57.3 | 3.861 | 0.01 | 0.941 | 0.058 | 0.0001 |
| 1e7 | 48.6 | 0.802 | 0.32 | 0.100 | 0.859 | 0.0029 | 57.2 | 3.441 | 0.01 | 0.932 | 0.066 | 0.0009 |
| 1e8 | 54.7 | 0.719 | 0.28 | 0.149 | 0.791 | 0.0107 | 57.2 | 3.040 | 0.05 | 0.800 | 0.166 | 0.0184 |
| 1e9 | 56.8 | 0.543 | 0.22 | 0.233 | 0.707 | 0.0179 | 57.2 | 2.690 | 0.05 | 0.820 | 0.151 | 0.0213 |
| 1e10 | 57.0 | 0.475 | 0.19 | 0.322 | 0.613 | 0.0266 | 57.1 | 2.360 | 0.06 | 0.810 | 0.160 | 0.0026 |
| 1e11 | 57.2 | 0.426 | 0.19 | 0.378 | 0.548 | 0.0365 | 57.3 | 2.130 | 0.09 | 0.820 | 0.140 | 0.0047 |
| 1e12 | 57.2 | 0.421 | 0.20 | 0.420 | 0.494 | 0.0500 | 57.3 | 2.110 | 0.01 | 0.984 | 0.016 | 0.0001 |

the central sphere of the proto-galaxies of mass M_L as a function of the age in two extreme cases of z_{for} , as indicated.

It is soon evident that, while some general trends can be recognized, there are also strong effects of the red-shift which in the present formulation of the problem are due to $T_{\text{CBR}}[z(t)]$. Recalling that M_p increases with the gas temperature, and decreases with the gas density and velocity dispersion, the final outcome will depend on the competition between these contrasting effects.

6.1. The reference case with $z_{\text{for}} = 5$

In the case of $z_{\text{for}} = 5$, soon after the initial stages M_p falls to the lowest permitted value of $0.1 M_\odot$. The early variations with time and galaxy mass are however sufficient to determine the different evolutionary histories of galaxies with different mass. The following remarks can be made

(i) In the very early stages of a galaxy, the temperature of the star forming gas though cooler than the current $T_{\text{CBR}} \simeq 18 \text{ K}$ is relatively low, and the mean gas density ρ_g and velocity dispersion Σ_g determine the starting value of M_p . Since they are lower and larger, respectively, in galaxies of high mass as compared to those of small mass, M_p is skewed towards more massive stars, and the slope of the IMF above M_p tends to flatten at increasing galaxy mass.

(ii) The energy from supernova explosions and stellar winds is injected into the interstellar gas making it hotter and hotter till a sort of equilibrium stage is reached, during which both the gas temperature and M_p remain nearly constant.

(iii) However, as star formation proceeds, the gas gets richer in metals thus increasing the cooling efficiency. The situation is eventually met in which cooling is so efficient that the gas temperature and peak mass of the IMF in turn start decreasing. This

implies that less energy is injected into the interstellar medium with consequent catastrophic fall-off of both temperature and peak mass to their limit values. These are the $T_{\text{CMBR}}[z(t)]$ and the associated M_p . In no case, however, M_p is let fall below $0.1 M_\odot$ (see Fig. 3).

(iv) The duration of this initial phase is longer at increasing mass of the proto-galaxy M_L , but in any case it is short compared to the total galaxy lifetime. However, it bears very much on the final outcome, because it determines the kind of stellar populations one would expect in galaxies of different mass.

(v) The overall duration of the star forming activity increases at decreasing galaxy mass *i.e.* $\Delta t_{\text{SF}} \propto M_L^{-1}$ as suggested by the abundance ratios $[\alpha/\text{Fe}]$.

(vi) As the central regions of a galaxy are denser than the external ones, we expect star formation to last longer over there.

6.2. The case of higher z_{for}

In the case of $z_{\text{for}} = 20$, the above trends are much different. In this case $T_{\text{CMBR}}[z(t)] \simeq 60$ K and the temperature dependence of M_p prevails. The peak mass starts and remains relatively high, and decreases only when metals provide enough cooling. However, the dependence of M_p on the gas density and velocity dispersion reverse the correlation with the galaxy mass: lower mass galaxies have the higher peak mass. Finally M_p falls to the limit value only after about 1 Gyr, *i.e.* much longer than in the previous case. Similar trends are found the other intermediate values of z_{for} .

6.3. Gas and metal ejection

As far as the contribution to metals and gas from the three zones of each galaxy we note the following:

(i) As expected, the bulk of metals are made in the central sphere and from this ejected in the form of winds. This holds independently of the galaxy mass and z_{for} . Looking at the galaxy with $M_L = 1 \times 10^9 M_\odot$, for $z_{\text{for}} = 5$ the fractionary amount of gas ejected by the central sphere at the stage of galactic wind is $M_g/M(R_e) = 0.011$, the rest is in stars and remnants ($M_s/M(R_e) = 0.942$), whereas the same galaxy if formed at $z_{\text{for}} = 20$ would expel $M_g/M(R_e) = 0.233$ and retain only $M_s/M(R_e) = 0.741$ in stars (the rest is in remnants).

(ii) The intermediate shell, though undergoing lighter stellar activity, is an important source of partially enriched gas. The typical gas fraction expelled by the intermediate shell is about $M_g/M(\Delta R)_i = 0.5-0.9$, with metallicities ranging from $Z=0.0001$ to $Z=0.02$. The rest of the mass is in stars and remnants.

(iii) The situation is even more extreme in the outermost corona, in which no significant star formation and metal enrichment take place. The gas is simply ejected back into the ICM.

Therefore, the outer regions of the proto-galaxies are the kind of engine we want, by which primordial gas is partially nuclearly processed without being fully converted into stars. In the section below we will better quantify the amounts of

material dispersed into the ICM by calculating the galactic ejecta of various elemental species.

The obvious criticism to these results is that they depend on the type of model used. While this may apply to the details, the main conclusion holds that given a certain amount of gas prone to become a galaxy only a fraction of it goes into stars, all the rest is dispersed back into the cluster medium after some nuclear processing has taken place.

This possibility is also supported by N-body Tree-SPH models of galaxy formation and evolution by Carraro et al. (in preparation), in which only about half of the initial baryonic mass of a galaxy (originally in form of gas) is turned into stars. All the rest is either dispersed to very large distances from the galactic center or ejected in form of galactic winds. Furthermore, these models show the highest fraction of gas turned into stars falls within the effective radius, whereas outside it little if none star formation occurs, in that much resembling our semi-analytical models.

The most important result of these calculations is that the standard one-zone models likely underestimate the effect of galactic wind.

7. Ejecta from galaxies

In the SDGW model, early on in the galaxy life the high rate of SN explosions supplies the gas with so much energy that despite the cooling mechanisms, the gas heats up to the stage at which its thermal energy exceeds the gravitational potential energy and the gas leaves the galaxy. From now on star formation stops and the rates of SN explosions (Type II first and Type I later) decline to small values. Shortly after the ejection of the galactic wind (say about 0.5 Gyr) the energy injection by SN explosion gets negligible small.

In the meantime, the stars formed during the previous active phase get old and eventually dye. When about 0.5 Gyr have elapsed, all massive stars have gone and stars of lower mass intervene (say $< 2 M_\odot$), whose fate is to become white dwarf after ejecting a fraction of their mass via quiet stellar winds. Therefore lots of gas are progressively accumulated in the galaxy. What is the fate of this gas?

Following the discussion by GM97, three post- t_{gw} scenarios have been envisaged:

(i) Continuous Type-Ia SN-driven winds up to the present. All gas liberated by stars after the wind phase is continuously ejected from galaxies. This possibility is not very likely because of the continuous decline in the energy supply by SN explosions.

(ii) Suppression of all the Ia-driven winds. All the gas liberated by stars is retained. The picture is extreme, but not to far from reality because most of the gas lost by stars has low kinetic energy, not enough to overwhelm the gravitational binding energy. Most likely the gas is heated up to the virial temperature of the galaxy and retained within the potential well of dark matter.

(iii) The so-called standard model in which the galactic wind phase stretches over a time interval of about 0.5–1 Gyr and then stops. The amount of gas expelled in the aftermath of the galactic

Table 4. Ejecta from galaxies with the IMF of Padoan et al. (1997) formed at different red-shifts z_{for} . These ejecta refer to the gas contained in the galaxy when the galactic wind driven by supernova explosions took place.

| z_{for} | M_L | M_g^{ej} | M_H^{ej} | M_O^{ej} | M_{Fe}^{ej} | M_g^{ej} | M_H^{ej} | M_O^{ej} | M_{Fe}^{ej} |
|------------------------|-------|------------|------------|------------|-------------------------------------|------------|------------|------------|---------------|
| Inner Sphere: $M(R_e)$ | | | | | Intermediate Shell: $M(\Delta R)_i$ | | | | |
| 20 | 1e6 | 1.35E+04 | 1.03E+04 | 2.62E+01 | 1.47E+01 | 1.78E+05 | 1.42E+05 | 1.24E+01 | 1.21E-01 |
| 20 | 1e7 | 4.14E+05 | 3.12E+05 | 2.00E+03 | 9.02E+02 | 1.76E+06 | 1.41E+06 | 1.22E+03 | 5.02E+01 |
| 20 | 1e8 | 6.17E+06 | 4.51E+06 | 6.99E+04 | 2.43E+04 | 1.53E+07 | 1.10E+07 | 3.37E+05 | 2.35E+04 |
| 20 | 1e9 | 9.65E+07 | 6.82E+07 | 2.01E+06 | 4.06E+05 | 1.57E+08 | 1.09E+08 | 3.54E+06 | 2.42E+05 |
| 20 | 1e10 | 1.33E+09 | 8.91E+08 | 4.02E+07 | 6.04E+06 | 1.77E+09 | 1.41E+09 | 4.50E+06 | 4.60E+05 |
| 20 | 1e11 | 1.56E+10 | 9.77E+09 | 5.86E+08 | 7.91E+07 | 1.77E+10 | 1.40E+10 | 6.01E+07 | 5.80E+06 |
| 20 | 1e12 | 1.74E+11 | 9.81E+10 | 7.76E+09 | 1.04E+09 | 1.86E+11 | 1.49E+11 | 1.27E+07 | 2.47E+06 |
| 15 | 1e6 | 4.64E+03 | 3.50E+03 | 3.07E+00 | 4.85E+00 | 1.74E+05 | 1.39E+05 | 2.02E+01 | 2.22E-01 |
| 15 | 1e7 | 9.19E+04 | 6.66E+04 | 1.29E+02 | 3.02E+02 | 1.72E+06 | 1.37E+06 | 1.31E+03 | 3.63E+01 |
| 15 | 1e8 | 9.85E+05 | 7.03E+05 | 3.78E+03 | 7.71E+03 | 1.44E+07 | 1.06E+07 | 2.70E+05 | 2.05E+04 |
| 15 | 1e9 | 1.63E+07 | 1.13E+07 | 2.32E+05 | 1.84E+05 | 1.69E+08 | 1.34E+08 | 6.45E+05 | 3.39E+04 |
| 15 | 1e10 | 8.16E+08 | 5.60E+08 | 2.04E+07 | 4.06E+06 | 1.77E+09 | 1.41E+09 | 3.38E+06 | 3.22E+05 |
| 15 | 1e11 | 1.12E+10 | 7.25E+09 | 3.71E+08 | 5.88E+07 | 1.76E+10 | 1.39E+10 | 5.06E+07 | 4.74E+06 |
| 15 | 1e12 | 1.33E+11 | 7.91E+10 | 5.45E+09 | 8.07E+08 | 1.86E+11 | 1.49E+11 | 9.80E+06 | 1.86E+06 |
| 10 | 1e6 | 1.16E+03 | 8.50E+02 | 2.85E-01 | 1.11E+00 | 1.64E+05 | 1.31E+05 | 4.07E+01 | 1.42E+00 |
| 10 | 1e7 | 1.85E+04 | 1.34E+04 | 7.50E+00 | 3.27E+01 | 1.27E+06 | 9.87E+05 | 1.12E+04 | 1.14E+03 |
| 10 | 1e8 | 5.01E+05 | 3.59E+05 | 7.55E+02 | 2.31E+03 | 1.32E+07 | 1.00E+07 | 1.78E+05 | 1.54E+04 |
| 10 | 1e9 | 6.54E+06 | 4.59E+06 | 3.99E+04 | 6.99E+04 | 1.71E+08 | 1.35E+08 | 6.40E+05 | 1.02E+05 |
| 10 | 1e10 | 1.28E+08 | 8.75E+07 | 2.18E+06 | 1.56E+06 | 1.76E+09 | 1.40E+09 | 2.71E+06 | 2.59E+05 |
| 10 | 1e11 | 3.32E+09 | 2.15E+09 | 1.00E+08 | 3.26E+07 | 1.75E+10 | 1.39E+10 | 5.38E+07 | 5.20E+06 |
| 10 | 1e12 | 5.26E+10 | 3.06E+10 | 2.22E+09 | 5.55E+08 | 1.86E+11 | 1.49E+11 | 6.53E+06 | 1.19E+06 |
| 5 | 1e6 | 7.33E+02 | 5.37E+02 | 1.33E-01 | 5.97E-01 | 1.10E+05 | 8.79E+04 | 9.57E+01 | 1.71E+01 |
| 5 | 1e7 | 9.36E+03 | 6.76E+03 | 3.31E+00 | 1.51E+01 | 1.18E+06 | 9.33E+05 | 3.96E+03 | 5.14E+02 |
| 5 | 1e8 | 2.24E+05 | 1.60E+05 | 2.16E+02 | 8.87E+02 | 1.11E+07 | 8.58E+06 | 9.24E+04 | 1.06E+04 |
| 5 | 1e9 | 4.47E+06 | 3.15E+06 | 1.68E+04 | 4.11E+04 | 1.74E+08 | 1.38E+08 | 2.35E+05 | 1.97E+04 |
| 5 | 1e10 | 7.95E+07 | 5.48E+07 | 1.00E+06 | 1.12E+06 | 1.76E+09 | 1.39E+09 | 5.39E+06 | 9.11E+05 |
| 5 | 1e11 | 2.21E+09 | 1.44E+09 | 6.36E+07 | 2.73E+07 | 1.75E+10 | 1.39E+10 | 9.91E+07 | 7.64E+06 |
| 5 | 1e12 | 5.09E+10 | 2.97E+10 | 2.18E+09 | 5.44E+08 | 1.85E+11 | 1.48E+11 | 8.43E+06 | 1.30E+06 |

Note: The ejecta from the outermost corona $M(\Delta R)_e$ are $M_g^{ej} = 0.397 \times M_L$, $M_H^{ej} = 0.8 \times 0.397 \times M_L$, $M_O^{ej} \simeq 0$ and $M_{Fe}^{ej} \simeq 0$.

wind is actually a sizable fraction of the large reservoir in the stars that have not yet reached their final stage. This is also confirmed by the calculation of GM97 and the little change in the total ejecta found passing from their minimal to maximal case.

In order to minimize the number of assumptions we limit ourselves to the most unfavorable yet realistic case: after the galactic wind episode, no slow gas ejection from galaxies takes place.

The mass of various elemental species (H, O, Fe) and total gas expelled by galaxies of different mass whose star forming history began at different red-shifts are presented in Table 4. The following notation is used: M_H^{ej} , M_O^{ej} , M_{Fe}^{ej} , and M_g^{ej} for the mass of hydrogen, oxygen, iron, and total gas (all in solar units). In presenting the data, distinction is made between the ejecta from the central sphere, the intermediate shell, and the outer corona for the sake of better understanding. However, when eventually using these data, the total ejecta will be the sum of all the components.

For the purpose of subsequent comparison, we also calculate ejecta from model galaxies of the same mass and same physical scheme, but with the assumption that the stellar IMF is always the Salpeter (1955) law given by Eq. (2). The results are presented in Table 5 with the same notation used in Table 4.

To give a quick idea of how the ejecta vary as a function of mass, red-shift z_{for} and type of IMF we plot in the two panels of Fig. 4 the sum of the ejecta M_{Fe}^{ej} (open triangles) and M_g^{ej} (filled squares) from the central sphere and intermediate shell obtained by using the IMF by PNJ97 (y-axis) and the classical Salpeter IMF (x-axis). The diagonal line is the locus where the two types of ejecta are equal. Moving from bottom-left to top-right in each panel the mass M_L of the proto-galaxy increases. The left and right panels are for $z_{for} = 5$ and $z_{for} = 20$, respectively. Firstly we note that at increasing M_L the IMF by PNJ97 tends to produce more Fe as compared to the Salpeter IMF and less Fe for low M_L . The cross-over mass M_L depends on the red-shift. Secondly, the gas ejecta are always nearly identical.

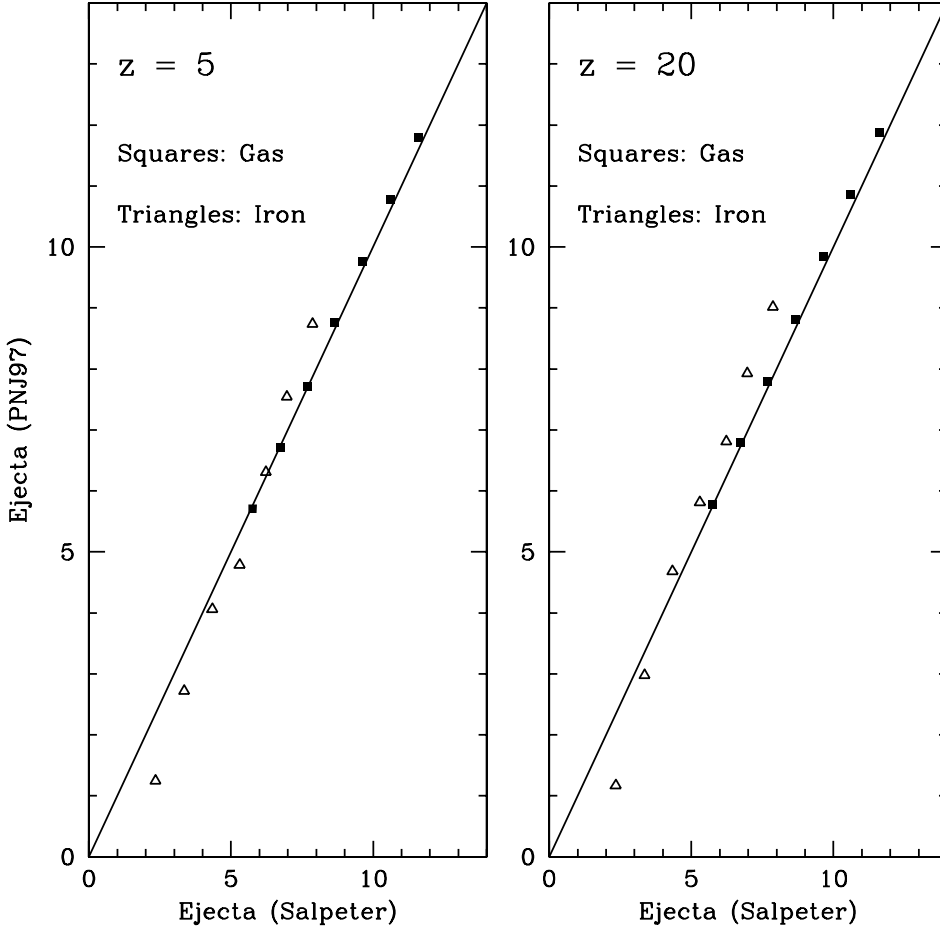


Fig. 4. Total amounts of $M_{\text{Fe}}^{\text{ej}}$ (open triangles) and M_{g}^{ej} (filled square) ejected by the central sphere and intermediate shell as a function of the proto-galaxy mass M_L , type of IMF, and red-shift z_{for} . The x-axis displays the ejecta with the Salpeter IMF, whereas the y-axis is the same but for the IMF by PNJ97. The plotted quantities are the logarithm of $M_{\text{Fe}}^{\text{ej}}$ and M_{g}^{ej} in solar units

Table 5. Ejecta from galaxies of different mass, whose IMF is the standard Salpeter law independently of the red-shift of galaxy formation. The ejecta refer to the stage of galactic wind and the gas present in the galaxy at that time. All masses are in solar units.

| M_L | M_{g}^{ej} | M_{H}^{ej} | M_{O}^{ej} | $M_{\text{Fe}}^{\text{ej}}$ |
|-------------------------------------|----------------------------|----------------------------|----------------------------|-----------------------------|
| Inner Sphere: $M(R_e)$ | | | | |
| 1e6 | 5.51E+04 | 3.64E+04 | 1.23E+03 | 1.89E+02 |
| 1e7 | 2.74E+05 | 1.73E+05 | 6.91E+03 | 1.75E+03 |
| 1e8 | 1.48E+06 | 9.15E+05 | 3.86E+04 | 1.54E+04 |
| 1e9 | 6.87E+06 | 4.23E+06 | 1.68E+05 | 1.21E+05 |
| 1e10 | 3.67E+07 | 2.34E+07 | 8.20E+05 | 8.33E+05 |
| 1e11 | 1.73E+08 | 1.12E+08 | 3.80E+06 | 4.05E+06 |
| 1e12 | 9.44E+08 | 6.13E+08 | 2.07E+07 | 3.11E+07 |
| Intermediate Shell: $M(\Delta R)_i$ | | | | |
| 1e6 | 1.19E+05 | 9.31E+04 | 6.10E+02 | 3.07E+01 |
| 1e7 | 1.02E+06 | 7.84E+05 | 8.95E+03 | 5.04E+02 |
| 1e8 | 7.60E+06 | 5.66E+06 | 9.80E+04 | 6.61E+03 |
| 1e9 | 4.88E+07 | 3.45E+07 | 8.65E+05 | 8.07E+04 |
| 1e10 | 2.93E+08 | 1.97E+08 | 6.25E+06 | 8.62E+05 |
| 1e11 | 1.59E+09 | 1.05E+09 | 3.12E+07 | 5.28E+06 |
| 1e12 | 8.37E+09 | 5.62E+09 | 41.40E+08 | 4.30E+07 |

Note: The ejecta from the outermost corona $M(\Delta R)_e$ are $M_{\text{g}}^{\text{ej}} = 0.397 \times M_L$, $M_{\text{H}}^{\text{ej}} = 0.8 \times 0.397 \times M_L$, $M_{\text{O}}^{\text{ej}} \simeq 0$ and $M_{\text{Fe}}^{\text{ej}} \simeq 0$.

Finally for the purpose of general use and sake of completeness we calculate the ejecta from dying stars all over the galaxy life from the stage of galactic wind to the present. We limit ourselves to the case of the IMF by PNJ97. The results are contained in Table 6 with the same notation as in the previous tabulations. By comparing the entries of Table 4 to those of Table 6 the following remarks can be made:

(i) The ejecta in stellar winds are always larger than the ejecta in the galactic wind.

(ii) The gas and heavy element ejecta in stellar winds from the inner sphere increase those by galactic wind roughly in equal proportions so that their inclusion would not alter the abundances of oxygen and iron.

(iii) The intermediate corona contributes to the yield of heavy elements more than in the previous phase, whereas it parallels the contribution to the gas. This can be explained by the different kind of IMF existing in the external regions. Owing to the lower gas density the IMF is indeed more skewed towards massive stars (see the entries of Table 3) and consequently it favors the production of Type II (and Type I) SN. Were these ejecta be included in the models, the final abundances would certainly change. However for the arguments given above this possibility seems to be unlikely.

Table 6. Total gas emitted by dying stars either in form SN explosions (type I and II) or quiet stellar winds since the time of galactic wind to the present. These quantities refer to the models with the IMF of Padoan et al. (1997).

| z_{for} | M_L | M_g^{ej} | M_H^{ej} | M_O^{ej} | $M_{\text{Fe}}^{\text{ej}}$ | M_g^{ej} | M_H^{ej} | M_O^{ej} | $M_{\text{Fe}}^{\text{ej}}$ |
|------------------------|-------|-------------------|-------------------|-------------------|-------------------------------------|-------------------|-------------------|-------------------|-----------------------------|
| Inner Sphere: $M(R_e)$ | | | | | Intermediate Shell: $M(\Delta R)_i$ | | | | |
| 20 | 1e6 | 1.07E+05 | 7.76E+04 | 5.75E+02 | 2.67E+03 | 9.00E+03 | 6.00E+03 | 5.46E+02 | 1.46E+02 |
| 20 | 1e7 | 1.71E+06 | 1.19E+06 | 1.51E+04 | 6.31E+04 | 1.00E+05 | 5.00E+04 | 6.97E+03 | 1.45E+03 |
| 20 | 1e8 | 1.67E+07 | 1.15E+07 | 2.24E+05 | 7.11E+05 | 2.00E+06 | 1.20E+06 | 6.60E+04 | 5.94E+04 |
| 20 | 1e9 | 1.47E+08 | 9.98E+07 | 2.56E+06 | 6.26E+06 | 1.70E+07 | 1.10E+07 | 5.90E+05 | 5.34E+05 |
| 20 | 1e10 | 1.28E+09 | 8.49E+08 | 2.83E+07 | 5.70E+07 | 1.20E+08 | 9.00E+07 | 3.01E+07 | 2.70E+06 |
| 20 | 1e11 | 1.15E+10 | 7.33E+09 | 3.02E+08 | 5.46E+08 | 1.20E+09 | 1.00E+09 | 3.09E+08 | 2.58E+07 |
| 20 | 1e12 | 1.03E+11 | 6.29E+10 | 3.24E+09 | 5.47E+09 | 2.00E+09 | 1.00E+09 | 2.93E+08 | 3.26E+07 |
| 15 | 1e6 | 6.25E+04 | 4.63E+04 | 2.62E+02 | 1.25E+03 | 1.10E+04 | 7.00E+03 | 4.44E+02 | 1.96E+02 |
| 15 | 1e7 | 1.15E+06 | 8.25E+05 | 8.07E+03 | 3.70E+04 | 1.20E+05 | 8.00E+04 | 6.61E+03 | 2.12E+03 |
| 15 | 1e8 | 1.22E+07 | 8.58E+06 | 1.22E+05 | 4.91E+05 | 2.60E+06 | 1.70E+06 | 7.00E+04 | 7.71E+04 |
| 15 | 1e9 | 1.31E+08 | 8.86E+07 | 2.11E+06 | 6.08E+06 | 2.00E+07 | 1.60E+07 | 2.62E+06 | 2.89E+05 |
| 15 | 1e10 | 1.31E+09 | 8.90E+08 | 2.48E+07 | 5.64E+07 | 1.20E+08 | 9.00E+07 | 3.18E+07 | 4.25E+06 |
| 15 | 1e11 | 1.22E+10 | 8.05E+09 | 2.83E+08 | 5.51E+08 | 1.30E+09 | 1.10E+09 | 2.94E+08 | 2.47E+07 |
| 15 | 1e12 | 1.13E+11 | 7.09E+10 | 3.15E+09 | 5.59E+09 | 2.00E+09 | 1.00E+09 | 2.58E+08 | 2.94E+07 |
| 10 | 1e6 | 2.78E+04 | 2.12E+04 | 7.81E+01 | 3.77E+02 | 1.60E+04 | 1.10E+04 | 2.69E+02 | 2.94E+02 |
| 10 | 1e7 | 4.33E+05 | 3.27E+05 | 1.52E+03 | 7.35E+03 | 3.80E+05 | 2.53E+05 | 5.90E+03 | 9.76E+03 |
| 10 | 1e8 | 7.78E+06 | 5.65E+06 | 4.96E+04 | 2.26E+05 | 3.30E+06 | 2.30E+06 | 6.30E+04 | 8.86E+04 |
| 10 | 1e9 | 9.16E+07 | 6.43E+07 | 9.90E+05 | 3.68E+06 | 1.80E+07 | 1.50E+07 | 2.63E+06 | 4.24E+05 |
| 10 | 1e10 | 1.05E+09 | 7.14E+08 | 1.72E+07 | 4.80E+07 | 1.30E+08 | 1.00E+08 | 3.26E+07 | 4.87E+06 |
| 10 | 1e11 | 1.17E+10 | 7.76E+09 | 2.53E+08 | 5.45E+08 | 1.40E+09 | 1.10E+09 | 2.92E+08 | 2.49E+07 |
| 10 | 1e12 | 1.17E+11 | 7.34E+10 | 3.39E+09 | 6.12E+09 | 2.00E+09 | 1.00E+09 | 2.09E+08 | 2.67E+07 |
| 5 | 1e6 | 2.23E+04 | 1.72E+04 | 4.79E+01 | 2.31E+02 | 3.20E+04 | 2.31E+04 | 1.53E+02 | 6.38E+02 |
| 5 | 1e7 | 2.83E+05 | 2.16E+05 | 7.96E+02 | 3.84E+03 | 3.30E+05 | 2.27E+05 | 2.64E+03 | 7.69E+03 |
| 5 | 1e8 | 4.71E+06 | 3.50E+06 | 2.23E+04 | 1.05E+05 | 3.80E+06 | 2.62E+06 | 4.36E+04 | 9.94E+04 |
| 5 | 1e9 | 7.08E+07 | 5.08E+07 | 6.03E+05 | 2.43E+06 | 1.50E+07 | 1.20E+07 | 3.26E+06 | 6.14E+05 |
| 5 | 1e10 | 9.10E+08 | 6.29E+08 | 1.32E+07 | 3.90E+07 | 1.30E+08 | 1.10E+08 | 2.94E+07 | 3.74E+06 |
| 5 | 1e11 | 1.12E+10 | 7.42E+09 | 2.43E+08 | 5.11E+08 | 1.40E+09 | 1.10E+09 | 2.89E+08 | 2.59E+07 |
| 5 | 1e12 | 1.15E+11 | 7.13E+10 | 3.56E+09 | 5.90E+09 | 3.00E+09 | 2.00E+09 | 1.76E+08 | 3.07E+07 |

Note: The ejecta from the outermost corona $M(\Delta R)_e$ are $M_g^{\text{ej}} \simeq 0$, $M_H^{\text{ej}} \simeq 0$, $M_O^{\text{ej}} \simeq 0$ and $M_{\text{Fe}}^{\text{ej}} \simeq 0$.

8. Modelling the ICM gas and metal contents

8.1. A reminder of the standard method

With knowledge of an elliptical's M_i^{ej} and V-band luminosity, the usual method is to integrate over the Schechter (1976) luminosity function. By normalizing to a cluster's luminosity L_V^E from its population of elliptical galaxies and introducing the luminosity L^* for the bright end of the luminosity function and the auxiliary variable $y = L_V/L_V^*$ one writes the total mass M_i^T of elemental species ejected into the ICM by galaxies of luminosity greater than L_V^{min}

$$\frac{M_i^T}{L_V^E} = \frac{\int_{y_{\text{min}}}^{\infty} M_i^{\text{ej}}(y)^\gamma \exp(-y) dy}{\int_{y_{\text{min}}}^{\infty} L_V y^\gamma \exp(-y) dy} \quad (10)$$

where γ is a suitable exponent and the ejecta are supposed to be functions of type $M_i^{\text{ej}}(\frac{L_V}{L_V^*})$. If the functions M_i^{ej} are power laws of the luminosity, then Eq. (10) reduces to a simple incomplete Γ -function as in MV88, Elbaz et al. (1995) and the case of *burst model* in Martinelli et al. (1999). More complex situations are not of interest here.

8.2. The new approach

The situation we want to deal with is more complex. First the ejecta M_i^{ej} are not simple power laws of M_L or luminosity, second they depend on z_{for} , third the mass range of galaxies we see today has likely varied with time (red-shift). Therefore, the straightforward use of the Schechter luminosity function can no longer be applied.

Based on these motivations, we prefer to follow a different approach whose essential steps are as follows:

(i) We start from the standard cosmological picture, in which the mass density of the Universe is dominated by collision-less Dark Matter, and structures in this component form from hierarchical gravitational clustering starting from small-amplitude, seed fluctuations, with smaller objects collapsing first and then merging to form larger and larger objects. Haloes of Dark Matter formed in this way yield the gravitational potential wells in which gas collects to form galaxies (Lacey & Cole 1993, 1994 and references therein). On the average, the proportion of Baryonic to Dark Matter is about 1:10.

(ii) In this context, the fraction Φ of mass in Dark Matter Haloes with mass M , at time t , per interval dM (Press & Schechter 1974; Lacey & Cole 1994) has the functional dependence

$$\frac{d\Phi}{dM} = \frac{1}{M} \left(\frac{2}{\pi}\right)^{1/2} \left(\frac{n+3}{6}\right) \left(\frac{M}{M^*}\right)^{\frac{(n+3)}{6}} \times \exp\left[-\frac{1}{2}\left(\frac{M}{M^*}\right)^{\frac{(n+3)}{3}}\right] \quad (11)$$

where M^* is the high-end cut-off mass, which in turn varies with the red-shift

$$M^* = M_{\text{Nor}} \times (1+z)^{-\frac{6}{n+3}} \quad (12)$$

The exponent n is the spectral index of the initial power spectrum of the perturbations. The mass M_{Nor} is here a free parameter used to fix the total mass in a cluster.

(iii) For the purposes of the present study, we will assume that at any time and hence red-shift, relations (11) and (12) also represent a sort of mass function for galaxies. In other words, we assume that the mass spectrum of proto-galaxies follows, albeit suitably scaled, the same distribution of Dark Matter. Based on this assumption, M^* acquires another meaning. Indeed, it can be conceived as the typical mass-scale of individual galaxies at any red-shift. In order to avoid confusion we will refer to it as M_L^* and name the corresponding M_{Nor} mass as M_{Nor}^L . For this latter, we assume the typical value of a galaxy with large mass, i.e. $M_{\text{Nor}}^L = 1 \times 10^{13} M_\odot$ at red-shift $z = 0$.

(iv) In addition to this, the following scenario for the bulk of stellar activity and hence gas ejection from galaxies of different total mass is envisaged. At any red-shift, lumps of gas with different mass reach the threshold condition for forming stars, do it on a relatively short time scale, and then cease because of the galactic wind mechanism. At any red-shift, there is suitable mass range within which this can occur. This is comprised between a minimum and maximum mass prone to collapse.

(v) Finally, since the galactic winds occur soon after the bulk of star formation has taken place, the so-called *instantaneous recycling* approximation can be adopted. Indeed looking at the entries of Table 3, t_{gw} is of the order of 0.7 Gyr or shorter. The approximation may not be fully adequate for galaxies ejecting the wind at high red-shift but it is acceptable for those doing it at low red-shift. In any case, preliminary calculations aimed at assessing the effect of taking into account the time delay between star formation and galactic wind show that the *instantaneous recycling* approximation is fully adequate for the purposes of this study.

Given these premises, the total mass in form of elemental species expelled by all galaxies of any mass and epoch of formation is

$$M_i^T = \int_{z_{\text{for}}}^0 \int_{M_L^{\text{min}}(z)}^\infty M_i^{\text{ej}} \frac{d\Phi[M_L, n, M_L^*(z)]}{dM_L} dM_L dz \quad (13)$$

where $M_i^{\text{ej}}(M_L, z)$ has its usual meaning,

Having adopted the Press-Schechter function as a sort of initial mass function for galaxies, one has to consider that this

function actually represents a mass aggregation process rather than hierarchical fragmentation of proto-clouds as in the case of the stellar IMF. In other words at any time a galaxy of mass M_L can either be the result of aggregating two galaxies of smaller mass that already had their stellar activity and consequent gas ejection phase in the past, or be an object undergoing star formation and gas ejection for the first time. The simplest way we can imagine to take this into account is that at any time (red-shift) only a fraction (say one half) of the galaxies with mass M_L are eligible to form stars and soon after eject gas. However, it is easy to understand that with the normalization procedure to be discussed below the above correction has no effect on the final results.

The problem now is to determine the lower integration limit M_L^{min} as a function of time (red-shift). The upper limit is less important because of the cut-off mass M_L^* in the exponential term so that extending the integration to a large value of the mass or even to ∞ for the sake of simplicity is acceptable.

Tegmark et al. (1997) have addressed the subject of the smallest mass size of the first cosmological objects, i.e. the minimum mass that a virialized gas cloud must have in order to be able to cool in the Hubble time. This minimum mass that is identified here with M_L^{min} is found to be strongly red-shift dependent, dropping from $10^6 M_\odot$ at $z \simeq 15$ to $10^3 M_\odot$ at $z \simeq 100$. From the results shown in their Fig. 6, we have derived the following analytical relations

$$M_L^{\text{min}} = 1.15 \times 10^{12} (1+z)^{-3.9} \quad \text{for } 15 \leq (1+z) \leq 30$$

$$M_L^{\text{min}} = 5.25 \times 10^9 (1+z)^{-1.9} \quad \text{for } 1 \leq (1+z) \leq 15$$

that are fully adequate to our purposes (M_L^{min} is in solar units).

Both M_L^* and M_L^{min} are plotted in Fig. 5 as a function of the red-shift z . The cut-off M_L^* mass plotted here is for $M_{\text{Nor}}^L = 10^{13} M_\odot$. At any red-shift, the mass interval comprised between M_L^{min} and M_L^* is the one most effective in enriching the ICM.

9. Normalization

Because of the arbitrariness of the mass scales involved, we need a procedure to normalize the results. With the aid of Eq. (13) we calculate the total mass stored into long-lived galaxies M_G^T , the total mass in gas ejected by these latter in form of galactic winds M_g^T and assume that their sum plus the total amount of primordial gas M_P left over by the galaxy forming process equals the present-day total baryonic mass M_B^T of a cluster. The mass of primordial gas M_P is expressed as a fraction of M_B^T , i.e. $M_P = \alpha M_B^T$. The normalization condition is

$$M_G^T + M_g^T + \alpha M_B^T = A_\alpha \times M_B^T \quad (14)$$

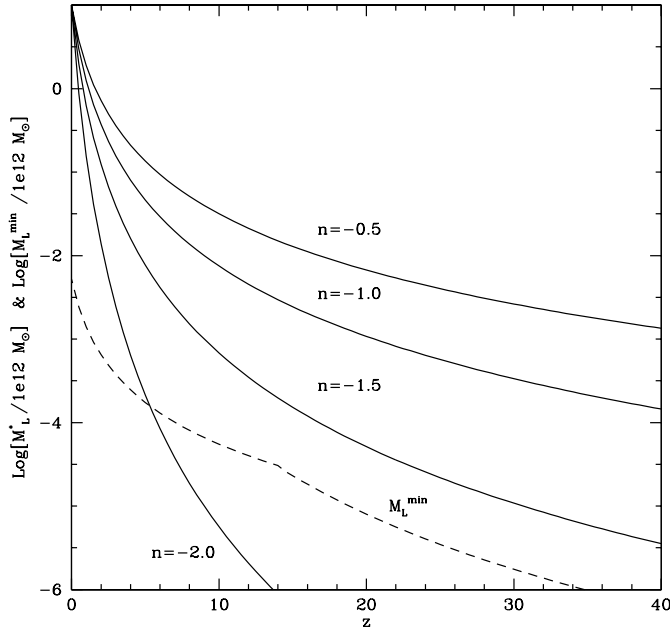
The constant A_α is used to scale all the results.

At this stage, we can proceed further assuming $\alpha=0$. Only at the very end of the analysis when comparing the theoretical results to the observational abundances we will re-normalize the results to cases with $\alpha \neq 0$.

The total mass in galaxies M_G^T is obtained by integrating the effective mass in stars M_G given by Eq. (6) over the Press-Schechter function of relation (13). The total masses M_g^T , M_O^T

Table 7. The galactic ejecta from MV88, MG95 and GM98. All masses are in solar units

| MV88 | | | | MG95 | | | GM98 | | |
|-------|---------------|---------------|------------|------------|---------------|------------|------------|---------------|------------|
| M_L | M_{Mg}^{ej} | M_{Fe}^{ej} | M_g^{ej} | M_O^{ej} | M_{Fe}^{ej} | M_g^{ej} | M_O^{ej} | M_{Fe}^{ej} | M_g^{ej} |
| 1E6 | | | | | | | 5.5E3 | 9.0E2 | 8.7E5 |
| 1E7 | | | | | | | 4.9E5 | 6.6E4 | 4.2E7 |
| 1E8 | | | | | | | | | |
| 1E9 | 3.2E5 | 1.8E6 | 4.8E8 | 5.5E6 | 2.9E5 | 3.5E8 | 1.9E7 | 1.6E6 | 7.8E8 |
| 1E10 | 1.6E6 | 1.8E6 | 1.8E9 | 2.9E7 | 3.3E6 | 9.4E8 | 7.8E8 | 8.0E7 | 2.8E10 |
| 1E11 | 1.2E7 | 1.6E8 | 1.1E10 | 6.8E7 | 2.3E7 | 1.8E9 | | | |
| 1E12 | 9.6E7 | 1.5E9 | 7.7E10 | 2.2E8 | 1.4E8 | 6.4E9 | 1.6E10 | 1.8E9 | 4.5E11 |
| 2E12 | 1.8E8 | 2.8E9 | 1.4E11 | 3.4E8 | 2.9E8 | 9.8E9 | | | |

**Fig. 5.** M_L^* and M_L^{\min} as a function of red-shift. The cut-off mass plotted here is for $M_{Nor}^L = 10^{13} M_\odot$, an extremely massive proto-galaxy

and M_{Fe}^T are derived in the same way by integrating the ejecta of Table 4 or Table 5 as appropriate.

Finally, the following values of the power spectrum index $n = -0.5, -1.0, -1.5, -2.0$, and $M_B^T = 10^{13}, 10^{14}, 10^{15}$, and $10^{16} M_\odot$ are considered.

10. Preliminary tests

10.1. Recovering previous results

Before proceeding further, we check whether the above method recovers the results obtained by other authors using galactic ejecta which are functions only of the galaxy mass and integrating their contributions over the Schechter luminosity function. To do so, we take the ejecta from MV88, MG95 and GM97 that are listed in Table 7, fix M_L^* to a typical present day value, drop the integration upon the red-shift in Eq. (13), assume the same normalization procedure as for the general case (with $\alpha=0$), and finally compare the results we get with those found by MV88,

MG95 and GM97. The comparison is shown in the left panel of Fig. 6, where the solutions for the ejecta by MV88 (left) and GM97 (right) are used. For this latter only the maximal ejecta are considered.

Like in Fig. 1, we correlate the total gas mass to the total iron mass. The filled triangles, squares, pentagons, and hexagons along the lines, correspond to the different choices for M_B^T we have made, i.e. $10^{13}, 10^{14}, 10^{15}$, and $10^{16} M_\odot$, respectively, and different values of the index n . The observational data for four clusters of different richness (MV88) are shown by the big empty squares and companion label. Finally, the open circles show the original solutions given by MV88 and GM97.

While as expected the theoretical results depend on M_B^T , the models slide up and down along the line of constant abundance, there is no significant dependence on the power spectrum n . Indeed each point is the superposition of four models, as many as the considered values of n .

It is soon evident that the two methods yield the same results within an acceptable tolerance. Indeed what matters here is that the solutions found by convolving in luminosity with the Schechter function fall along the line given by convolving in mass with the Press-Schechter function.

The main conclusion is that the method we have adopted leads to results that are fully consistent with those based on the usual integration upon the luminosity function.

10.2. Varying the galaxy models and IMF

As already recalled, our model galaxies are conceived as three zones systems, i.e. a inner sphere where most of star formation and chemical enrichment occurs, an intermediate shell in which some star formation and chemical enrichment takes place, and a third outermost corona in which in practice no stars and metals are made. This scheme is a consequence of the SDGW model we have adopted. The ejecta from the three regions have therefore different chemical composition. The outermost zone in particular expels back into the ICM virtually primordial gas.

To fully understand the effect of the galaxy models in usage, we examine here how the results change passing from the one-zone to the three-zone description. To this purpose one-zone galaxy models are calculated for both types of IMF (Salpeter and PNJ97). No details are given here for the sake of brevity.

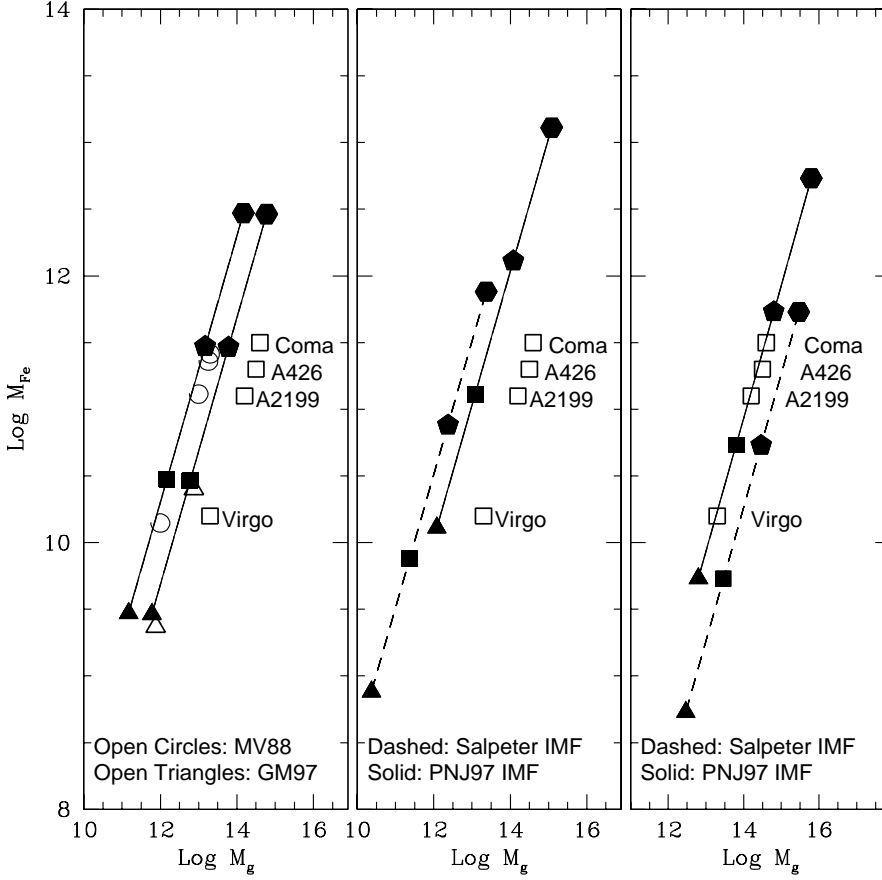


Fig. 6. Left Panel: Recovering old results with the mass integration method. The ejecta are from MV88 and GM97 as indicated. The IMF is the Salpeter law. While all the previous results are all recovered, the discrepancy between theory and data is still there. Middle Panel: One-zone galaxy models with the Salpeter (dashed line) and IMF by PNJ97 (solid line). Right Panel: the effect of the three-zone structure and IMF. The new ejecta from three-zone models much alleviate the problem. The variable IMF, in particular, yields results that fairly agree with the observations. In all the panels: the filled triangles, squares, pentagons and hexagons correspond to M_B^T equal to $10^{13} M_\odot$, $10^{14} M_\odot$, $10^{15} M_\odot$, and $10^{16} M_\odot$, respectively. See the text for more details

Models of this type are much similar to those calculated by MG95 and/or GM97 but for details.

Also in this case, we start with the simplest scheme in which no dependence on the red-shift is considered. In the case of the IMF by PNJ97, we adopt the models with $z_{\text{for}}=5$ as the reference case. The procedure is the same as above. The results are shown in the middle and right panels of Fig. 6 for the one-zone and three-zones models, respectively. The analysis is made both for the IMF of Salpeter and PNJ97.

Firstly, the one-zone models predict too little gas at given iron content. The situation is worse for the Salpeter IMF, whereas it gets better with the IMF by PNJ97. Secondly, the three-zone models yield more gas at given iron production. Finally, the same models with the IMF by PNJ97 remarkably agree with the data.

Given these premises, we may safely proceed further and look for the effect of using more complex model galaxies, with different stellar IMFs, ejecta, and finally epoch of bulk stellar activity.

11. Total amounts of iron and gas injected into the ICM

We then let M_L^* and galactic ejecta vary with the red-shift and make use of the complete Eq. (13). Table 8 contains the total amount of iron, oxygen and gas injected into the ICM as functions of several key parameters, i.e. the power spectrum n , the normalization baryonic mass M_B^T , the kind of stellar IMF, and

the galactic ejecta (galaxy model in turn). All these models are calculated with $\alpha=0$ (no primordial gas is left over).

For the sake of better understanding, we also consider the reference case with the Salpeter IMF, in which the only dependence on the red-shift is via M_L^* and M_L^{min} , both for the one-zone and the three-zones model galaxies. The comparison of these solutions with the corresponding ones discussed in the previous section, allows us to single out the sole effect of M_L^* , and M_L^{min} , i.e. the mass function of galaxies.

Therefore in Table 8 three groups of models are displayed: (i) Case A are models with the one-zone description and the Salpeter IMF. (ii) Case B models have the same IMF but they are based on the three-zones scheme in order to better mimic a real situation. (iii) Finally, Case C models have the IMF by PNJ97 and the three-zone structure.

The theoretical results for the three cases are shown in Fig. 7 and compared to the observational data. The meaning of the various symbols is the same as in Fig. 6.

We note that models A (dotted symbols) predict too low a gas content of the ICM, i.e. they suffer from the long known disagreement. The situation is the opposite for models B (dashed symbols). They eject too much gas for the amount of expelled iron. Finally we have models of type C which nicely fit the data. The large difference between Cases A and B simply resides in the outermost corona of case B which contains large quantities of gas and no metals.

Table 8. The total mass of gas, iron and oxygen injected by galaxies into the ICM for different combinations of the power spectrum n , the normalization mass for the baryonic component M_B^T , the stellar IMF, and the type of ejecta. All the data refer to the normalization constant A for $\alpha=0$ (A_0). All masses are in solar units.

| n | A_0 | M_B^T | M_G^T | M_g^T | M_H^T | M_O^T | M_{Fe}^T | [O/H] | [Fe/H] | [O/Fe] |
|--|------------|---------|----------|----------|----------|----------|------------|-----------|-----------|-----------|
| Case A: One-Zone Models with the Salpeter IMF and $\alpha=0$. | | | | | | | | | | |
| -0.5 | 4.4333(e0) | 1.0E+13 | 9.89E+12 | 1.15E+11 | 7.65E+10 | 2.10E+09 | 8.02E+08 | 3.04E-01 | 6.02E-01 | -2.98E-01 |
| -0.5 | 4.4333(e1) | 1.0E+14 | 9.89E+13 | 1.15E+12 | 7.65E+11 | 2.10E+10 | 8.02E+09 | 3.04E-01 | 6.02E-01 | -2.98E-01 |
| -0.5 | 4.4333(e2) | 1.0E+15 | 9.89E+14 | 1.15E+13 | 7.65E+12 | 2.10E+11 | 8.02E+10 | 3.04E-01 | 6.02E-01 | -2.98E-01 |
| -0.5 | 4.4333(e3) | 1.0E+16 | 9.89E+15 | 1.15E+14 | 7.65E+13 | 2.10E+12 | 8.02E+11 | 3.04E-01 | 6.02E-01 | -2.98E-01 |
| -2.0 | 4.4608(e1) | 1.0E+13 | 9.90E+12 | 9.99E+10 | 6.67E+10 | 1.76E+09 | 7.58E+08 | 2.87E-01 | 6.37E-01 | -3.50E-01 |
| -2.0 | 4.4608(e2) | 1.0E+14 | 9.90E+13 | 9.99E+11 | 6.67E+11 | 1.76E+10 | 7.58E+09 | 2.87E-01 | 6.37E-01 | -3.50E-01 |
| -2.0 | 4.4608(e3) | 1.0E+15 | 9.90E+14 | 9.99E+12 | 6.67E+12 | 1.76E+11 | 7.58E+10 | 2.87E-01 | 6.37E-01 | -3.50E-01 |
| -2.0 | 4.4608(e4) | 1.0E+16 | 9.90E+15 | 9.99E+13 | 6.67E+13 | 1.76E+12 | 7.58E+11 | 2.87E-01 | 6.37E-01 | -3.50E-01 |
| Case B: Three-Zone Models with the Salpeter IMF and $\alpha=0$. | | | | | | | | | | |
| -0.5 | 4.1766(e0) | 1.0E+13 | 5.88E+12 | 4.12E+12 | 3.28E+12 | 2.18E+09 | 8.14E+08 | -1.31E+00 | -1.02E+00 | -2.88E-01 |
| -0.5 | 4.1766(e1) | 1.0E+14 | 5.88E+13 | 4.12E+13 | 3.28E+13 | 2.10E+10 | 8.14E+09 | -1.31E+00 | -1.02E+00 | -2.88E-01 |
| -0.5 | 4.1766(e2) | 1.0E+15 | 5.88E+14 | 4.12E+14 | 3.28E+14 | 2.10E+11 | 8.14E+10 | -1.31E+00 | -1.02E+00 | -2.88E-01 |
| -0.5 | 4.1766(e3) | 1.0E+16 | 5.88E+15 | 4.12E+15 | 3.28E+15 | 2.10E+12 | 8.14E+11 | -1.31E+00 | -1.02E+00 | -2.88E-01 |
| -2.0 | 4.0177(e1) | 1.0E+13 | 5.90E+12 | 4.10E+12 | 3.27E+12 | 1.80E+09 | 7.63E+08 | -1.39E+00 | -1.05E+00 | -3.42E-01 |
| -2.0 | 4.0177(e2) | 1.0E+14 | 5.90E+13 | 4.10E+13 | 3.27E+13 | 1.80E+10 | 7.63E+09 | -1.39E+00 | -1.05E+00 | -3.42E-01 |
| -2.0 | 4.0177(e3) | 1.0E+15 | 5.90E+14 | 4.10E+14 | 3.27E+14 | 1.80E+11 | 7.63E+10 | -1.39E+00 | -1.05E+00 | -3.42E-01 |
| -2.0 | 4.0177(e4) | 1.0E+16 | 5.90E+15 | 4.10E+15 | 3.27E+15 | 1.80E+12 | 7.63E+11 | -1.39E+00 | -1.05E+00 | -3.42E-01 |
| Case C: Three-Zone Models with the IMF by PNJ97 and $\alpha=0$. | | | | | | | | | | |
| -0.5 | 5.8347(e0) | 1.0E+13 | 3.70E+12 | 6.30E+12 | 4.94E+12 | 2.05E+10 | 5.05E+09 | -5.15E-01 | -4.09E-01 | -1.07E-01 |
| -0.5 | 5.8347(e1) | 1.0E+14 | 3.70E+13 | 6.30E+13 | 4.94E+13 | 2.05E+11 | 5.05E+10 | -5.15E-01 | -4.09E-01 | -1.07E-01 |
| -0.5 | 5.8347(e2) | 1.0E+15 | 3.70E+14 | 6.30E+14 | 4.94E+14 | 2.05E+12 | 5.05E+11 | -5.15E-01 | -4.09E-01 | -1.07E-01 |
| -0.5 | 5.8347(e3) | 1.0E+16 | 3.70E+15 | 6.30E+15 | 4.94E+15 | 2.05E+13 | 5.05E+12 | -5.15E-01 | -4.09E-01 | -1.07E-01 |
| -2.0 | 5.6127(e1) | 1.0E+13 | 3.68E+12 | 6.32E+12 | 4.95E+12 | 2.10E+10 | 5.26E+09 | -5.06E-01 | -3.92E-01 | -1.14E-01 |
| -2.0 | 5.6127(e2) | 1.0E+14 | 3.68E+13 | 6.32E+13 | 4.95E+13 | 2.10E+11 | 5.26E+10 | -5.06E-01 | -3.92E-01 | -1.14E-01 |
| -2.0 | 5.6127(e3) | 1.0E+15 | 3.68E+14 | 6.32E+14 | 4.95E+14 | 2.10E+12 | 5.26E+11 | -5.06E-01 | -3.92E-01 | -1.14E-01 |
| -2.0 | 5.6127(e4) | 1.0E+16 | 3.68E+15 | 6.32E+15 | 4.95E+15 | 2.10E+13 | 5.26E+12 | -5.06E-01 | -3.92E-01 | -1.14E-01 |

The reasons for the easier agreement with the IMF by PNJ97 are (i) the copious amounts of gas with mild yet significant chemical enrichment that is ejected back into the ICM by the intermediate shell corona of galaxies of any mass, and (ii) the larger amounts of gas (now significantly enriched in metals) ejected by galaxies of any mass when they are let form stars at high red-shift and therefore under an IMF skewed towards more massive stars.

Furthermore, the total mass in galaxies and gas varies passing from Case A to Case B and finally, Case C models. While in Cases A and B the mass in galaxies is larger than the mass in gas, in Case C models the mass in galaxies is about half of that in gas.

Furthermore, it is worth noticing the relatively marginal role played by the power spectrum index n in all the above properties.

However before drawing conclusions from the M_g vs M_{Fe} plane about which galaxy model (stellar IMF) is at work, we examine the present-day abundances of Fe and O and their evolution with the red-shift.

12. Present-day iron and oxygen abundances

The entries of Table 8 display the abundances [O/H], [Fe/H] and [O/Fe] expected in the ICM at the present time in the hypothesis that no primordial gas is left over by the galaxy forming activity.

With the IMF by PNJ97 the abundances are $\langle [O/H] \rangle = -0.511$, $\langle [Fe/H] \rangle = -0.401$, and $\langle [O/Fe] \rangle = -0.111$, whereas with the Salpeter IMF and the three-zones models, the abundances are $\langle [O/H] \rangle = -1.35$, $\langle [Fe/H] \rangle = -1.03$, and $\langle [O/Fe] \rangle = -0.315$. Finally, with the Salpeter IMF and the one zone description we get $\langle [O/H] \rangle = 0.296$, $\langle [Fe/H] \rangle = 0.620$, and $\langle [O/Fe] \rangle = -0.324$.

As expected the present day abundances significantly vary with the IMF in usage. The Salpeter IMF predicts super-solar or sub-solar abundances depending on the type of galaxy models. In any case, their abundance ratios are one third solar. In contrast the IMF by PNJ97 predicts sub-solar abundances and nearly solar abundance ratios.

Finally, there is no dependence on the total baryonic mass M_B^T as observed, and a very little one on the power spectrum index n .

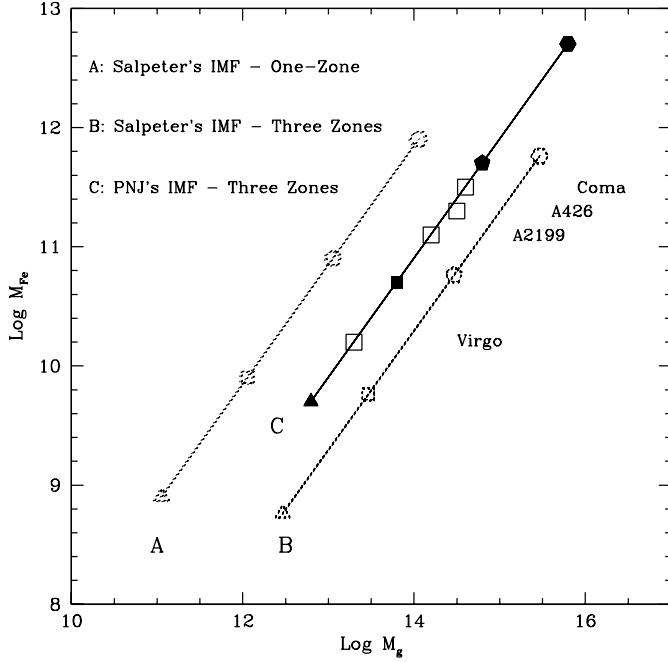


Fig. 7. Comparison of the iron-gas mass relationship for galaxies with the Salpeter (dotted lines) and the IMF by PNJ97 (solid line). The meaning of the symbols is the same as in Fig. 6

Table 9 compares the present results with those obtained in previous studies, limited to $[\text{Fe}/\text{H}]$ and $[\text{O}/\text{Fe}]$. The following remarks can be made:

(i) One-zone model galaxies predict values of $[\text{Fe}/\text{H}]$ that are higher than the mean observational estimate $[\text{Fe}/\text{H}] = -0.542$ (see below). The GM97-min models are those getting closer to the observational value.

(ii) The multi-zone models of MMC99 also predict $[\text{Fe}/\text{H}]$ values that are much higher than the mean observational estimate. These models are indeed calculated with a Salpeter-like IMF and resemble those of our Case A.

(iii) Only case C models predict values of $[\text{Fe}/\text{H}]$ very close but yet not equal to the observational determination.

(iv) The $[\text{O}/\text{Fe}]$ ratio is less of a problem, because all models predict values that are compatible with the observational estimate.

A provisional conclusion from this comparison is that only galaxy models with multi-zone structure and the IMF by PNJ97 can yield results in close agreement with the data.

13. Cosmological evolution of the ICM

Due to the continuous ejection from galaxies of different mass, the iron and oxygen contents steadily increase at decreasing red-shift toward the present-day values.

For the sake of illustration, in Fig. 8 we show the Case B model with $M_B^T = 10^{15} M_\odot$ and $n = -1.5$. Similar trends occur for all the other values of M_B^T and n . These quantities refer to the sole component ejected by galaxies and do not take into account the effect of pristine material. Therefore they do

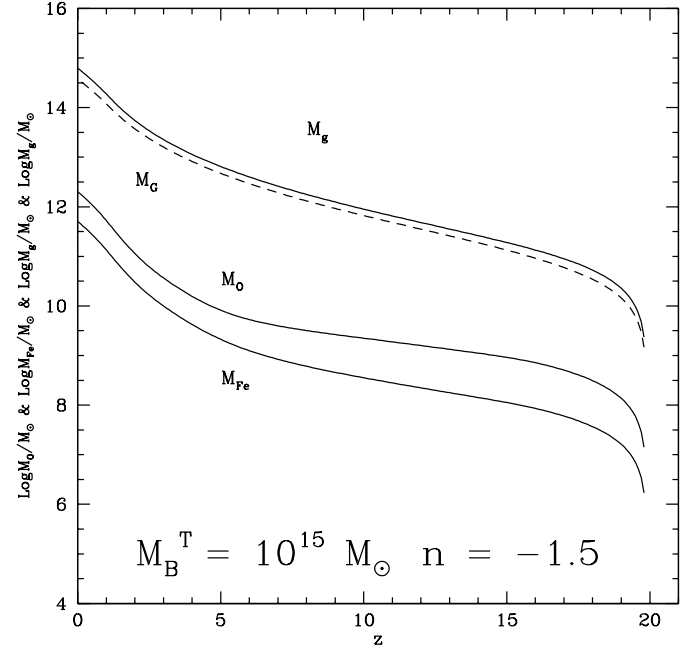


Fig. 8. The variation of M_O^T , M_{Fe}^T and M_g^T ejected by galaxies into the ICM and the mass M_G^T locked up in galaxies as a function of the red-shift for the case with $M_L^* = 10^{13} M_\odot$, $M_B^T = 10^{15} M_\odot$ and $n = -1.5$

Table 9. Present day abundances from different studies

| Source | [Fe/H] | | [O/Fe] | |
|------------|--------|-------|--------|-------|
| MV88 | 0.53 | 0.65 | | |
| GM97 (min) | -0.17 | | | |
| GM97 (max) | 0.16 | | | |
| MMC99 (a) | 0.22 | 0.36 | -0.33 | 0.27 |
| MMC99 (b) | 0.75 | 0.90 | -0.12 | -0.04 |
| C2000 (A) | 0.60 | 0.64 | -0.30 | -0.35 |
| C2000 (B) | -1.05 | -1.02 | -0.29 | -0.34 |
| C2000 (C) | -0.41 | -0.39 | -0.11 | -0.10 |

MV88: one-zone models; GM97 (min): one-zone models and minima ejecta; GM97 (max): one-zone models and maxima ejecta; MMC99 (a): one-zone models; MMC99 (b): multi-zone models; C2000 this paper.

not represent the variation of the ICM abundances with the red-shift.

Before comparing with observational data for clusters at different red-shift one has to consider that the material ejected from galaxies is diluted by the primordial gas likely present in the cluster. In other words one has to develop a model for the chemical evolution of the ICM. In the following we proposed a very simple scheme for the chemical evolution of the ICM.

At any age (red-shift) the primordial gas content of a cluster is continuously consumed by galaxy formation. A fraction of the used up material is locked for ever in the long lived stellar content of a galaxy, whereas the rest is given back to the ICM both in form of newly synthesized heavy elements and original

material. Basing on these simple considerations we may write the following conservation equations for the three elemental species of interest here, namely hydrogen, oxygen and iron.

Oxygen and iron are simply generated by galaxies, therefore their values at any red-shift z are given by Eq. (13), whereby the integration over the red-shift goes from z_{for} to z (see for instance the curves of Fig. 8). The current total mass of these elements are indicated by $M_{\text{O}}^{\text{T}}(z)$ and $M_{\text{Fe}}^{\text{T}}(z)$. As for the current total mass hydrogen, $M_{\text{H}}^{\text{T}}(z)$, this is the difference between the initial value $X_{\text{P}} M_{\text{B}}^{\text{T}}$ (with X_{P} the primordial abundance $X_{\text{P}} = 0.8$) and the quantity locked up into the long-lived stars of galaxies, i.e. $M_{\text{G}}^{\text{T}}(z)$,

$$M_{\text{H}}^{\text{T}}(z) = X_{\text{P}} M_{\text{B}}^{\text{T}} - M_{\text{G}}^{\text{T}}(z) \quad (15)$$

The three quantities above are functions of the normalization constant, i.e. of the fraction α of the primordial gas still present today. Recalling that the calculations have been performed for $\alpha = 0$, all the quantities in question must be re-scaled if other choices for α in the range from 0 to 1 are made. It is an easy matter to show that the following relations hold

$$M_{\text{Fe}}^{\text{T}}(z)_{\alpha} = (1 - \alpha) M_{\text{Fe}}^{\text{T}}(z)_0 \quad (16)$$

$$M_{\text{O}}^{\text{T}}(z)_{\alpha} = (1 - \alpha) M_{\text{O}}^{\text{T}}(z)_0 \quad (17)$$

$$M_{\text{H}}^{\text{T}}(z)_{\alpha} = X_{\text{P}} M_{\text{B}}^{\text{T}} - (1 - \alpha) M_{\text{G}}^{\text{T}}(z)_0 \quad (18)$$

from which the abundances of Fe and O with respect to red-shift can be easily derived for any value of α .

In Fig. 9 we compare the abundance ratio $X_{\text{Fe}}/X_{\text{Fe},\odot}$ predicted by the above relations for the models with $M_{\text{B}}^{\text{T}} = 10^{15} M_{\odot}$ and $n = -1.5$ (top panel) and $n = -0.5$ (bottom panel) with the values measured in several clusters at different red-shifts. The filled circles are the data by Mushotzky & Loewenstein (1997), and the four open squares are the data for the clusters in Table 1.

Most of the discussion below applies to both panels. Looking at the case with $n = -1.5$, the solid, heavy line corresponds to the Case C model with $\alpha=0$ (no primordial gas exists today). The present value of the iron abundance is $\langle X_{\text{Fe}}/X_{\text{Fe},\odot} \rangle = 0.45$. This is about 40% higher than the mean value of observational data ($\langle X_{\text{Fe}}/X_{\text{Fe},\odot} \rangle = 0.276$).

The consequences of this comparison are straightforward. If one wants to bring Case C models to match the mean observational value one has to dilute the galaxy ejecta with primordial gas which in this case should amount to about 20% ($\alpha = 0.2$). This case is shown by the thin solid line.

With the Salpeter IMF and the one-zone description (Case A) there are such a shortage of gas and large production of iron that formal agreement with the observational data is possible only diluting the ejecta by a factor of 14, which means that the vast majority of the ICM gas ought to be primordial, a long known result in literature. With the three-zones description and $\alpha = 0$ (Case B), for nearly the same amounts of expelled iron as before, we get $\langle X_{\text{Fe}}/X_{\text{Fe},\odot} \rangle = 0.25$ which is somewhat lower than but still marginally compatible with the mean observational

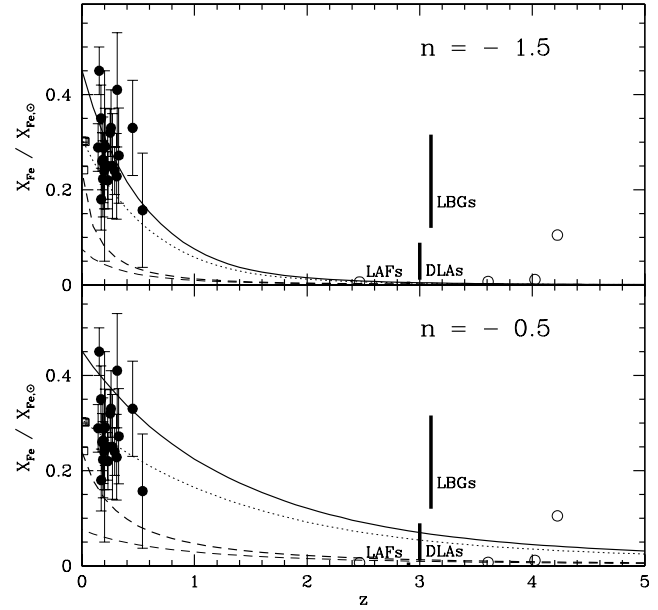


Fig. 9. The variation of the abundance $X_{\text{Fe}}/X_{\text{Fe},\odot}$ as a function of the red-shift expected for models with $M_{\text{B}}^{\text{T}} = 10^{15} M_{\odot}$ and $n = -1.5$ (top panel) and $n = -0.5$ (bottom panel). The filled circles are the data by Mushotzky & Loewenstein (1997). The open squares are the four clusters of Table 1. The heavy solid line is the evolution of Case C models, the thin dotted line is the same but with the addition of 20% of primordial gas left over at the present time ($z = 0$). The heavy dashed line is the prediction of Case B models, and finally the thin dashed line is the same but with the addition of 20% of primordial gas. The vertical bars show the metallicity range of damped Ly- α systems (DLAs), Ly-break galaxies (LBGs) and Ly- α forest (LAFs). Data from Pettini (2000). The open circles are the data for DLAs by Prochaska & Wolfe (2000)

determination, whereas with $\alpha = 0.2$ we get $\langle X_{\text{Fe}}/X_{\text{Fe},\odot} \rangle = 0.15$ which is definitely too low.

All the models predict the abundance ratio $\langle X_{\text{Fe}}/X_{\text{Fe},\odot} \rangle$ to decrease with red-shift. The decrease is, however, much milder and within the range of the observational data for C models, whereas it is much stronger and well below the data for models of Case B. Furthermore, the rapidity with which these curves decline at increasing red-shift is also function of the power spectrum index n . They tend to flatten at increasing n (see the bottom panel of Fig. 9).

The results of Case C with $n = -1.5$ are particularly interesting because, in the red-shift interval 0 to 0.5, they predict mean iron abundances from 0.45 to 0.2 $X_{\text{Fe},\odot}$ for $\alpha = 0$, and 0.3 to 0.15 $X_{\text{Fe},\odot}$ for $\alpha = 0.2$. The latter estimates are not too far from value of 1/10 $X_{\text{Fe},\odot}$ given by Renzini (2000 and references) basing on completely independent arguments.

Finally, the observational data show a large scatter likely reflecting real differences in the iron abundances. With the Salpeter IMF there is no leverage because for any value of α they run too low compared with the data (and the IMF is constant). With the IMF by PNJ97, the agreement is within the uncertainty of the observational data, α may change from cluster to cluster, and the finally the IMF itself may vary from case to case..

Are the results of Fig. 7 and Fig. 9 suggesting that the solution with the IMF by PNJ97 ought to be preferred?

The answer to this question could perhaps come from data at higher red-shift, say in the range 1 to 3, which to our knowledge are not yet available for the ICM. Chemical abundances have been determined for damped Ly- α systems DLA (see Matteucci et al. 1997; Pettini et al. 1997; Lu et al. 1996, 1998; Prochaska & Wolfe 2000, and references therein), Ly-break galaxies LBG (see Pettini 2000 for a review), and the Ly- α forest LAF (see Savaglio 1998). The picture which is emerging is that at high red-shift ($z=3$), there is a large spread in metallicity. Ranking objects as a function of their metal content on log scale with respect to solar, shortly indicated by $[m/H]$, the following schematic trend appears $-3.0 \leq [m/H]_{LAF} \leq -2.0$, $-2.0 \leq [m/H]_{DLA} \leq -1$, and $-1.0 \leq [m/H]_{LBG} \leq -0.5$. The above ranges are indicated in Fig. 9 by the vertical bars. These are artificially displaced in the range $2.8 \leq z \leq 3$ for the sake of clarity. Lu et al. (1998) provide estimates of $[Fe/H]$ in DLAs between $1 \leq z \leq 3$: they range from -2 to -1 with a weak tendency to decrease at increasing z . Remarkably, while LAFs and DLAs tend to be as metal rich as the ICM, the LBGs have higher metallicities. The reason for that is not clear.

Data in the range $0.8 < z < 2$ should perhaps help to discriminate among the various possibilities. Finally, better modeling of the chemical evolution of the ICM is required. Work is in progress to provide such a model (Moretti, Portinari & Chiosi, in preparation).

14. Summary and conclusions

In this paper we have presented theoretical estimates of the total amounts of gas and heavy elements (iron and oxygen) expected in the ICM of galaxy clusters as a consequence of the SDGW mechanism.

The analysis stands on several important assumptions and changes with respect to previous studies:

(i) Multi-zone galaxy models yield a more realistic description of the ejecta in which the effects of gradients in star formation and chemical enrichment are taken into account.

(ii) The adoption of an IMF which varies with the physical conditions of the star forming medium. The action resides in the systematic shift of the peak mass of the IMF with the gas temperature. Since no cooling process exists decreasing the temperature of a galaxy's gas below the limit set by the current value of the CBR, the immediate consequence follows that the IMF of proto-galaxies whose stellar activity began at high red-shift (when the CBR temperature was higher than the present-day one of molecular clouds) is different from the one in galaxies which did the same but at lower red-shift.

(iii) The mass range of star forming proto-galaxies is also let depend on red-shift. According to current understanding of this problem the minimum mass for a galaxy prone to collapse within the Hubble time decreases at increasing red-shift. As far as the maximum mass is concerned this is supposed to follow the same functional dependence of the mass-scale for Dark Matter aggregation in the Press-Schechter formalism.

(iv) The basic assumption is made that at any time (red-shift) the mass distribution of proto-galaxies follows the same law as for Dark Matter, however with masses comprised between the current minimum and maximum values. This is equivalent to assuming a sort of continuously varying mass function for galaxies as well. The time (red-shift) dependence is through M_L^{\min} and M_L^* .

(v) Individual galaxies are supposed to evolve and undergo the SDGW episode in isolation, neglecting any effect by the surrounding medium. Galaxy ejecta are calculated at the SDGW stage, ignoring the fate of all the gas that is later introduced into the intergalactic medium by dying stars. It is most likely that the largest fraction of this gas is actually retained by the galaxy lacking a strong source of energy able to power a sort of steady galactic wind. It seems reasonable to suppose that this gas emitted by stars at low velocities (say 30 to 60 km/s) is heated up to the virial temperature of the whole galaxy and remains bound to it in the potential well of dark matter.

(vi) It is found that models based on the IMF by PNJ97 predict total amounts of iron, gas and absolute abundance of Fe and abundance ratios that are fully compatible with observational determination. However even in this case some dilution (up to about 20%) by primordial gas (never cycled through galaxies) is required. This is less than the 80%–90% proposed by MV88, the 65% estimated by GM97 and Ferreras & Silk (1999), and finally the factor of about ten invoked by MMC99.

(vii) The adoption of the IMF by PNJ97 is not a strictly unavoidable condition for the success of the proposed scheme. Any other IMF of the type given by Eq. (3) would lead to similar results provided the mass scale M_s varies with the physical conditions, more precisely increases with the temperature, of the star forming medium. Many physical arguments suggest that indeed this is the case. See the discussion presented in Sect. 4.

(viii) The weak sensitivity of the results to the power spectrum index n or in other words the slope of the Press-Schechter function can be understood by considering that the convolution of galaxy ejecta with the galaxy mass function determines a suitable range of galaxy masses mostly contributing to the total ejecta. Similar results are found also in previous analyses where the Schechter luminosity function is used.

(ix) The adoption of the multi-zone scheme, though much improving on the final result, is not enough to solve the problem if not accompanied by an IMF of the type we have adopted. This is shown by the high Fe abundance obtained with the multi-zone models of MMC99 in which a Salpeter-like IMF has been adopted.

(x) Finally, we have proposed simple model for the chemical evolution of the ICM, which despite its crudeness, predicts abundances of the ICM in clusters located at different red-shifts that are in satisfactory agreement with the observational data.

Despite the many uncertainties in galaxy and galaxy cluster evolution, the results we have obtained perhaps suggest that the problem is set on the right track.

Acknowledgements. I wish to acknowledge the friendly hospitality and stimulating environment provided by MPA in Garching where this paper has been completed during leave of absence from the Astronomy Department of the Padua University. I also like to thank Laura Portinari for her constructive criticism and valuable comments. This study has been financially supported by the Italian Ministry of University, Scientific Research and Technology (MURST) under contract "Formazione ed evoluzione delle galassie" n. 9802192401.

References

- Anders E., Grevesse N., 1989, *Geochimica et Cosmochimica Acta* Vol. 53, 197
- Arimoto N., Matsushita K., Yshimaru Y, Osaki T., Renzini A., 1997, *ApJ* 477, 128
- Arnaud M., Rothenflug R., Boulade O., Vigroux L., Vangioni-Flamm E., 1992, *A&A* 254, 49
- Bower R.G., Lucey J.R., Ellis R.S., 1992, *MNRAS* 254, 601
- Bressan A., Chiosi C., Fagotto F., 1994, *ApJS* 94, 63
- Bressan A., Chiosi C., Tantalo R., 1996, *A&A* 311, 425
- Canizares C.R., Marert T.H., Donahue M.E., 1988, In: Fabian A.C. (ed.) *Cooling Flows in Clusters and Galaxies*. Kluwer, Dordrecht, p. 63
- Chiosi C., 2000, In: Hubeny I., Heap S.R., Cornett R.H. (eds.) *Spectrophotometric Dating of Stars and Galaxies*. ASP Conf. Ser. Vol. 192, p. 251
- Chiosi C., Bressan A., Portinari L., Tantalo R., 1998, *A&A* 339, 355
- Ciotti L., D'Ercole A., Pellegrini S., Renzini A., 1991, *ApJ* 376, 380
- David L.P., Forman W., Jones C., 1991, *ApJ* 380, 39
- De Propriis R., Pritchett C.J., Harris W.E., McClure R.D., 1995, *ApJ* 450, 534
- Elbaz D., Arnaud M., Vangioni-Flam E., 1995, *A&A* 303, 345
- Ferreras I., Silk J., 1999, *ApJ* in press, astro-ph/9910385
- Finoguenov A., David L.P., Ponman T.J., 1999, *ApJ* submitted, astro-ph/9908150
- Fukazawa Y., Makishima K., Tamura T., et al., 1998, *PASJ* 50, 187
- Gibson B.K., 1996, *MNRAS* 278, 829
- Gibson B.K., Matteucci F., 1997, *ApJ* 475, 47
- Ishimaru Arimoto N., 1997, *PASJ* 49, 11
- Lacey C., Cole S., 1993, *MNRAS* 262, 627
- Lacey C., Cole S., 1994, *MNRAS* 271, 676
- Larson R.B., 1974, *MNRAS* 166, 585
- Larson R.B., 1995, *MNRAS* 272, 213
- Larson R.B., 1998, *MNRAS* 301, 569
- Lu L., Sargent W.L.W., Barlow T.A., Churchill C.W., Voght S.S., 1996, *ApJS* 107, 475
- Lu L., Sargent W.L.W., Barlow T.A., 1998, *AJ* 115, 55
- Martinelli A., Matteucci F., Colafrancesco S., 1998, *MNRAS* 298, 42
- Martinelli A., Matteucci F., Colafrancesco S., 1999, astro-ph/99051138, MMC99
- Matteucci F., 1997, *Fund. Cosmic Phys.* 17, 283
- Matteucci F., Gibson B.K., 1995, *A&A* 304, 11
- Matteucci F., Vettolani G., 1988, *A&A* 202, 21
- Matteucci F., Molaro P., Vladilo G., 1997, *A&A* 321, 45
- Mihara K., Takahara F., 1994, *PASJ* 46, 447
- Mushotzky R.F., Holt S.S., Smith B.W., Boldt E.A., 1981, *ApJ* 225, 21
- Mushotzky R.F., Loewenstein M., 1997, *ApJ* 481, L63
- Mushotzky R.F., Loewenstein M., Arnaud M., et al., 1996, *ApJ* 466, 686
- Nath B.B., Chiba M., 1995, *ApJ* 454 604
- Padoan P., Nordlund A.P., Jones B.J.T., 1997, *MNRAS* 288, 145, PNJ97
- Pettini M., 2000, astro-ph/0001075
- Pettini M., King D. L., Smith L.J., Hunstead R.W., 1997, *ApJ* 478, 536
- Press W.H., Schechter P., 1974, *ApJ* 187, 425
- Prochaska J.X., Wolfe A.M., 2000, *ApJ* 533, L5
- Renzini A., 1997, *ApJ* 488, 35
- Renzini A., 2000, astro-ph/0001312
- Renzini A., Ciotti L., D'Ercole A., Pellegrini S., 1993, *ApJ* 419, 52
- Rothenflug R., Arnaud M., 1985, *A&A* 144, 431
- Rothenflug R., Vigroux L., Mushotzky R.F., Holt S.S., 1984, *ApJ* 279, 53
- Salpeter E.E., 1955, *ApJ* 121, 161
- Sarazin C.L., 1979, *Astrophys. Lett.* 20, 93
- Sarazin C.L., 1986, *Rev. Mod. Phys.* 58, 1
- Savaglio S., 1998, *AJ* 116, 1055
- Scalo J., 1998, In: Gilmore G., Howell D. (eds.) *The Initial Mass Function*. ASP Conf. Ser. Vol. 142, p. 201
- Schechter P., 1976, *ApJ* 488, 35
- Tantalo R., Chiosi C., Bressan A., Fagotto F., 1996, *A&A* 311, 361
- Tantalo R., Chiosi C., Bressan A., 1998, *A&A* 333, 419
- Tegmark M., Silk J., Rees M.J., et al., 1997, *ApJ* 474, 1
- Tinsley B.M., 1980, *Fund. of Cosmic Phys.* 5, 287
- Trentham N., 1994, *Nat* 372, 157
- Vazdekis A., Casuso E., Peletier R.F., Beckman J.E., 1996, *ApJS* 106, 307
- Young P.J., 1976, *AJ* 81, 807
- White R.E. III, 1991, *ApJ* 367, 69
- White R.E. III, 1999, *MNRAS* in press, astro-ph/9909467
- White R.E. III, Dupke R.A., 2000, astro-ph/0001304
- White S.D.M., Navarro J.F., Evrard A.E., Frenk C., 1993, *Nat* 366, 429
- Whorthey G., Dorman B., Jones L.A., 1996, *AJ* 112, 948